

# Coupled Climate Model Simulation of Tropical–Extratropical Cloud Bands over Southern Africa

RACHEL JAMES

*Climate Research Lab, Oxford University Centre for the Environment, Oxford, United Kingdom, and  
Department of Oceanography, University of Cape Town, Cape Town, South Africa*

NEIL C. G. HART AND CALLUM MUNDAY

*Climate Research Lab, Oxford University Centre for the Environment, Oxford, United Kingdom*

CHRIS J. C. REASON

*Department of Oceanography, University of Cape Town, Cape Town, South Africa*

RICHARD WASHINGTON


*Climate Research Lab, Oxford University Centre for the Environment, Oxford, United Kingdom*

(Manuscript received 3 October 2019, in final form 12 June 2020)


## ABSTRACT

There are increasing efforts to use climate model output for adaptation planning, but meanwhile there is often limited understanding of how models represent regional climate. Here we analyze the simulation in global coupled climate models of a key rainfall-generating mechanism over southern Africa: tropical temperate troughs (TTTs). An image-processing algorithm is applied to outgoing longwave radiation data from satellites and models to create TTT event sets. All models investigated produce TTTs with similar circulation features to observed. However, there are large differences among models in the number, intensity, and preferred longitude of events. Five groups of models are identified. The first group generates too few TTTs, and relatively dry conditions over southern Africa compared to other models. A second group generates more TTTs and wet biases. The contrast between these two groups suggests that the number of TTTs could explain intermodel variations in climatological rainfall. However, there is a third group of models that simulate up to 92% more TTTs than observed, but do not have large rainfall biases, as each TTT event is relatively weak. Finally, there are a further two groups that concentrate TTTs over the subcontinent or the ocean, respectively. These distinctions between models are associated with the amount of convective activity in the Congo Basin, the magnitude of moisture fluxes into southern Africa, and the degree of zonal asymmetry in upper-level westerly flow. Model development focused on tropical convection and the representation of orography is needed for improved simulation of TTTs, and therefore southern African rainfall.

---

 Denotes content that is immediately available upon publication as open access.

---

 Supplemental information related to this paper is available at the Journals Online website: <https://doi.org/10.1175/JCLI-D-19-0731.s1>.

---

*Corresponding author:* Rachel James, [rachel.james@ouce.ox.ac.uk](mailto:rachel.james@ouce.ox.ac.uk)

## 1. Introduction

The importance of preparing for future climate change is increasingly being recognized, and there are mounting efforts to incorporate climate projections into adaptation planning (Hewitt et al. 2012; Vaughan and Dessai 2014; Hewitson et al. 2017; Nissan et al. 2019). Yet, in many cases, there is still relatively limited understanding of simulated changes in future climate. The availability of climate model data greatly exceeds the capacity of the

DOI: 10.1175/JCLI-D-19-0731.1

© 2020 American Meteorological Society. For information regarding reuse of this content and general copyright information, consult the [AMS Copyright Policy](https://www.ametsoc.org/PUBSReuseLicenses) ([www.ametsoc.org/PUBSReuseLicenses](https://www.ametsoc.org/PUBSReuseLicenses)).

scientific community to analyze and understand it, and there has been insufficient research into the fidelity with which global models simulate regional climates. This is particularly true for climate regions within Africa (James et al. 2018), where, until very recently, none of the global climate models was developed (Watterson et al. 2014).

While modeling centers routinely assess their new model versions, and there are efforts to rank and compare models globally (e.g., Gleckler et al. 2008; Reichler and Kim 2008; Schaller et al. 2011; Watterson et al. 2014), this evaluation is not always sufficient to understand how models simulate regional processes of variability and change. To achieve that, more work is needed to analyze the processes relevant to each region (James et al. 2018). And, since climate change will most prominently be experienced through changes in the distribution of extreme events (IPCC 2012), it is particularly important to investigate climate models' simulation of weather systems (Tennant 2003).

Southern Africa is one region that warrants greater research attention. Many reports have highlighted agreement between climate models that southern Africa will become drier in future (World Bank 2012; Collins et al. 2013; Niang et al. 2014). However, climate models generally simulate too much rainfall over this region, therefore the future reduction of this precipitation is somewhat questionable (James and Washington 2013; Munday and Washington 2018, 2019). Furthermore, the consensus between model projections occurs during the drier seasons, but in austral summer, the main rainy season for most of southern Africa, there is a marked variation in historical precipitation climatologies (Lazenby et al. 2016; Munday and Washington 2017) as well as divergence of future rainfall among climate models (Shongwe et al. 2009; James et al. 2014). This divergence implies differences in models' representation of regional climate processes, and the weather systems which contribute to the rainfall climatology. If projections are to be useful for adaptation planning, it is therefore important to investigate how the models represent southern African weather.

Tropical–extratropical cloud bands, known regionally as tropical temperate troughs (TTTs), contribute a large proportion of summer rainfall over subtropical southern Africa (Washington and Todd 1999; Harrison 1984; Tozuka et al. 2014), particularly heavy rainfall (Todd and Washington 1998; Hart et al. 2013; Manhique et al. 2011, 2015). TTTs extend diagonally northwest to southeast between tropical convective regions and upper-tropospheric waves in the midlatitude westerlies. They are an important feature of all three Southern Hemisphere convergence zones. The South Pacific and South Atlantic convergence zones are the most pronounced and present all year. The south Indian convergence zone (SICZ) is evident over

southern Africa, Madagascar, and the southern Indian Ocean during austral summer (Hart et al. 2018a). TTTs in the SICZ interact with convection in the Congo Basin, storm tracks in the Southern Ocean, the St. Helena and Mascarene highs, and the Angola low (Todd et al. 2004; Fauchereau et al. 2009; Hart et al. 2010; Ratna et al. 2013; Macron et al. 2014), and their frequency varies interannually, particularly during El Niño–Southern Oscillation events (Fauchereau et al. 2009; Hart et al. 2018a). Any future change in regional circulation has potential to alter the frequency, location, and intensity of TTTs, with important implications for precipitation. A key step in assessing and understanding climate projections over southern Africa is therefore diagnosing whether and how well climate models simulate TTTs.

Previous work has examined TTTs in global and regional climate models (Vigaud et al. 2012; Tozuka et al. 2014; James et al. 2018; Hart et al. 2018b), but, to the authors' knowledge, no previous study has analyzed their occurrence in the models that are the most commonly used for future climate projection: the Coupled Model Intercomparison Project (CMIP) ensemble. In this paper, the representation of TTTs over southern Africa is analyzed in models from phase 5 of CMIP (CMIP5; Taylor et al. 2012). While CMIP6 data are gradually becoming available (Eyring et al. 2016), including the first global model developed in Africa (Bopape et al. 2019), CMIP5 models are still (in 2020) the most commonly used for climate projection, impact, and adaptation work.

The aim of the paper is to characterize the representation of TTTs in CMIP5: Can the models generate TTTs with similar dynamics to those observed? Do models produce TTTs with a similar climatological frequency and location? When TTTs occur in models, do they have similar implications for regional precipitation? In answering these questions, the paper is designed to inform the use of models in decision-making: to help interpret modeled outcomes, and to put future projections in the context. The paper also seeks to inform model development, by exploring processes associated with intermodel divergence and biases in simulated TTTs relative to observations. Since TTTs also occur in the South Pacific and South Atlantic convergence zones, the work also has potential to deliver insights useful for other parts of the Southern Hemisphere.

The paper is arranged as follows. The next section provides an overview of the CMIP5 model runs and satellite and reanalysis datasets. The third section outlines the methods used to identify and compare TTTs. An automated cloud band identification algorithm (Hart et al. 2012) is applied to daily outgoing longwave radiation (OLR) data, generating an event set of TTTs for

TABLE 1. CMIP5 models, grid spacing, and variables used in this study.

Model	Atmospheric resolution		Data availability							
			Daily						Monthly	
	Latitude (°)	Longitude (°)	OLR	Pr	$u$	$v$	$q$	$\omega$	zg	$T$
ACCESS1.0	1.25	1.88	x	x	x	x	x	x	x	x
ACCESS1.3	1.25	1.88	x	x	x	x	x	x	x	x
BCC-CSM1.1-m	2.79	2.81	x	x	x	x	x	x	x	x
BNU-ESM	2.79	2.81	x	x	x	x	x	x	x	x
CanESM2	2.79	2.81	x	x	x	x	x	x	x	x
CMCC-CESM	3.44	3.75	x	x	x	x	x	x	x	x
CMCC-CM	0.75	0.75	x	x	x	x	x	x	x	x
CMCC-CMS	1.86	1.88	x	x	x	x	x	x	x	x
CNRM-CM5	1.40	1.41	x	x	x	x	x	x	x	x
CSIRO-Mk3.6.0	1.87	1.88	x	x	x	x	x	x	x	x
FGOALS-g2	2.79	2.81	x	x	x	x	x	x	x	x
GFDL CM3	2	2.5	x	x	x	x	x		x	x
GFDL-ESM2G	2.02	2	x	x	x	x	x	x	x	x
GFDL-ESM2M	2.02	2.5	x	x	x	x	x	x	x	x
HadGEM2-CC	1.25	1.88	x	x	x	x	x		x	x
HadGEM2-ES	1.25	1.88	x	x					x	x
INM-CM4	1.5	2	x	x	x	x	x		x	x
IPSL-CM5A-LR	1.89	3.75	x	x	x	x	x	x	x	x
IPSL-CM5A-MR	1.27	2.5	x	x	x	x	x	x	x	x
IPSL-CM5B-LR	1.89	3.75	x	x	x	x	x	x	x	x
MIROC5	1.40	1.41	x	x	x	x	x	x	x	x
MIROC-ESM	2.79	2.81	x	x	x	x	x	x	x	x
MIROC-ESM-CHEM	2.79	2.81	x	x	x	x	x	x	x	x
MPI-ESM-LR	1.87	1.88	x	x	x	x	x	x	x	x
MPI-ESM-MR	1.87	1.88	x	x	x	x	x	x	x	x
MRI-CGCM3	1.12	1.13	x	x	x	x	x	x	x	x
NorESM1-M	1.89	2.5	x	x	x	x	x	x	x	x

each model. This event set is used to investigate three research questions, which are addressed in turn. First (section 4), do models generate TTTs with similar circulation features to observed? Second (section 5), how do the number, location, and intensity of TTTs compare between models, and how do these characteristics relate to precipitation biases? Third (section 5), what factors are associated with differences in the modeled number, frequency, and intensity of TTTs? The paper closes with a summary and conclusions.

## 2. Data

The analysis is based on data from 27 CMIP5 models, which are compared to satellite and reanalysis data, as a best estimate of the contemporary climate system. A 35-yr period was used for the analysis: 1970–2004 for CMIP5 models, and 1979–2013 for satellite and reanalysis data.

### a. Climate model data

Data were downloaded from the CMIP5 archive, for “historical” simulations, run with observed atmospheric forcings up to 2005. All models with daily OLR data

were used (see Table 1), and the first run for each model was selected (“r1i1p1”). As well as OLR data, the following data were downloaded where available: orography data (orog), daily precipitation (pr), and daily vertical velocity ( $\omega$ ), specific humidity ( $q$ ), zonal wind ( $u$ ) and meridional wind ( $v$ ) on pressure levels, monthly geopotential height (zg), and temperature ( $T$ ) on pressure levels (Table 1). Analyses were conducted on each model at native resolution. The most recent complete 35-yr period was extracted: 1970–2004.

### b. Satellite and reanalysis datasets

Daily mean OLR data are from the National Oceanic and Atmospheric Administration (NOAA) Climate Data Record (hereafter NCDR-OLR for short) (Lee et al. 2011; Lee 2014). These data are based on high-resolution infrared radiation satellite data and are available at a  $1^\circ \times 1^\circ$  resolution from 1979 to present. Precipitation data are from TRMM 3B42 version 7 (hereafter simply TRMM), which is a merged satellite and rain gauge daily dataset, at  $0.25^\circ \times 0.25^\circ$  resolution, available for 1997–2014 (Huffman et al. 2007, 2014). Circulation ( $u$ ,  $v$ ,  $\omega$ ) and humidity ( $q$ ) data on pressure levels were extracted from reanalysis

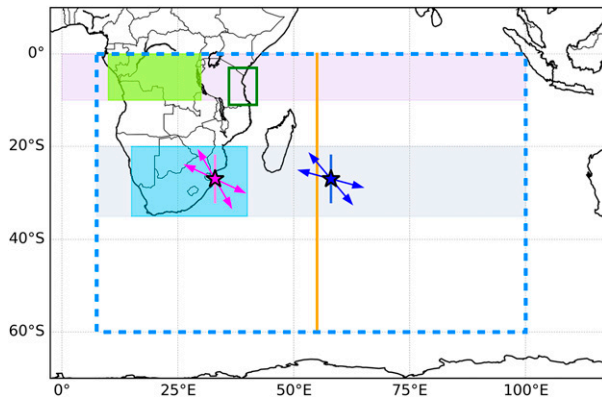


FIG. 1. Overview of domains and coordinates used in the paper. The blue dashed line shows the full domain used for the MetBot analysis. Pink and blue stars show the centroid longitudes used for continental and Madagascan samples, respectively, with vertical lines to indicate the range of centroid latitudes and arrows to show the range of orientations. The orange line is used to divide continental from Madagascan TTTs. Blue, gray, and green shaded boxes indicate areas averaged to represent subtropical southern Africa, the subtropics, and the southern Congo Basin. The purple shaded region is used to analyze tropical OLR. The dark green box shows the domain over which winds are averaged to calculate the Froude number.

datasets, and the figures in the paper show data from the European Centre for Medium-Range Weather Forecasts (ECMWF) interim reanalysis (ERA-Interim, hereinafter ERAI; ECMWF 2009; Dee et al. 2011), analyzed at  $0.75^\circ \times 0.75^\circ$  resolution. Analyses have also been repeated with the National Centers for Environmental Prediction–Department of Energy (NCEP–DOE) second Atmospheric Model Intercomparison Project (AMIP-II) reanalysis (NCEP2) (Kanamitsu et al. 2002), yielding qualitatively consistent results. All satellite and reanalysis datasets (except TRMM) were analyzed for 1979–2013, as a recent and commonly available 35-yr period. A 16-yr period (1998–2013) was analyzed from TRMM. In selecting these time periods, data availability was prioritized. As the CMIP runs are uninitialized, exact correspondence with the time period selected for models was not required.

### 3. Identification and comparison of daily weather systems

TTTs were identified in each dataset using an automated cloud band identification algorithm (“MetBot”), developed by Hart et al. (2012, 2018a). Contiguous regions of low OLR that have sufficient latitudinal extent and positive tilt (northwest–southeast orientation) are flagged as tropical–extratropical cloud bands, or TTTs. Data from the days previous to and following flagged days are analyzed to characterize the life cycle of the

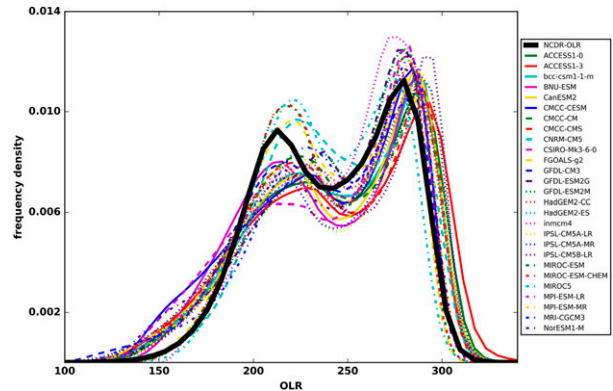


FIG. 2. Histograms of daily OLR data ( $\text{W m}^{-2}$ ) for grid points  $7.5^\circ\text{--}100^\circ\text{E}$ ,  $0^\circ\text{--}60^\circ\text{S}$  for satellite (thick black line) and model (colored lines) historical time periods.

TTT event and track its movement. Here the software was applied to a large domain ( $7.5^\circ\text{--}100^\circ\text{E}$ ,  $0^\circ\text{--}60^\circ\text{S}$ ; blue dashed line in Fig. 1) over southern Africa and the southwest Indian Ocean, encompassing the SICZ region and extending from the equator to the midlatitudes to capture tropical–extratropical interaction.

A key step in the algorithm is the identification of low OLR values, a proxy for high convective cloud. A threshold is used to distinguish “low” and “high” OLR. In applying the MetBot to satellite data, Hart et al. (2012) determined the threshold by plotting the distribution of daily OLR values for all the grid boxes in the full domain, yielding a bimodal distribution with a low OLR peak and a high OLR peak (Fig. 2), and then a value in the saddle of this distribution was selected ( $240 \text{ W m}^{-2}$ ), slightly above the low OLR peak. Given that CMIP5 models have slight differences in underlying OLR distributions (Fig. 2), in applying the software to this model ensemble, the threshold was defined objectively for each model using a downhill simplex algorithm to specify the saddle of the bimodal distribution. All analysis was also repeated with thresholds set at  $5 \text{ W m}^{-2}$  higher and lower, to test the sensitivity of the findings to this parameter, and results were found to be robust (see S1 and S2 in the online supplemental material).

An event set of TTTs was generated for each model, including cloud band coordinates, the longitude and latitude of the centroid, the cloud band’s angle of orientation, the date of occurrence, and the longevity of the event in days. This event set enables investigation of the weather conditions and circulation features associated with each cloud band, facilitating analysis of the first research question: Do models generate TTTs with similar circulation features to observed? The event set is also used to generate statistics to investigate the second and third research questions, which rely on quantification of the number,

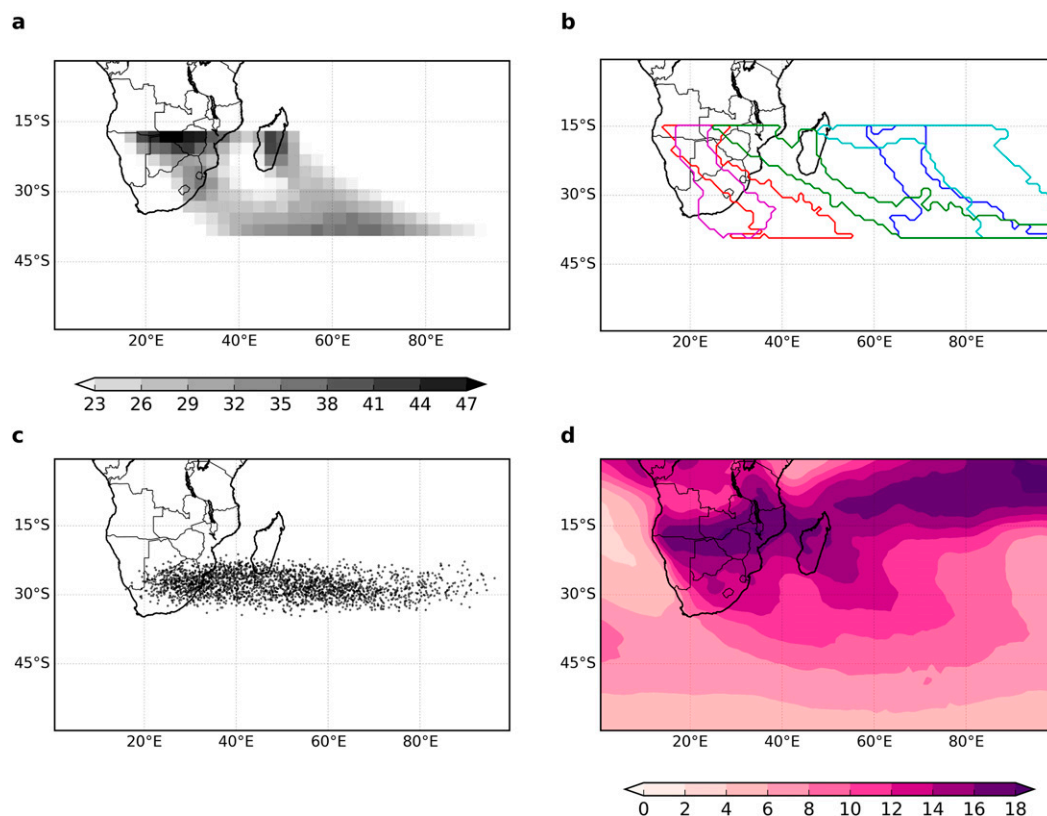


FIG. 3. Variation of daily TTTs observed in satellite data (NCDR-OLR) during NDJFM. (a) Spatial distribution of TTTs, based on the percentage of TTT days when a TTT cloud band covers each box in a  $2.5^\circ \times 2.5^\circ$  grid, (b) five randomly selected examples of TTT outlines, (c) TTT centroids, and (d) coefficient of variation of OLR values on all TTT days (%).

location, and intensity of TTTs. The event set includes data for the full year, but this paper focuses on November to March (NDJFM), the austral summer season, when the majority of TTTs occur (Hart et al. 2013).

*a. Using subsets of commonly located TTTs to compare modeled circulation features to observed*

Comparing circulation features between the satellite and modeled event sets is challenging due to the inherent synoptic variability in TTTs. As illustrated in Fig. 3, each TTT in nature has a different morphology, location, and intensity. Figure 3b illustrates examples of cloud band outlines generated from the event set. Figure 3a shows that, while there are two preferential zones of TTT activity (as identified in previous literature; Harrison 1984; Hart et al. 2012), one extending southeastward from southern Africa and one extending from Madagascar, most locations in the SICZ have a TTT overhead on  $<30\%$  of TTT days. The full range of TTT locations, illustrated by the centroids in Fig. 3c, is large, extending from the Namib coast to the central Indian Ocean. There is also large variation in the OLR

values on TTT days, particularly at the southern edge of tropical Africa (Fig. 3d).

The synoptic variability in observed TTTs means it is difficult to evaluate consistency between simulated and natural events. Figure 4 shows the distribution of TTTs from each model, demonstrating a large range of TTT locations, and highlighting the challenge of comparing circulation features between datasets. We address this challenge by extracting a subset of TTTs with common location and orientation. By focusing on TTTs which have similar latitude, longitude, and tilt, we can meaningfully analyze similarities and differences between models in terms of the associated circulation, including upper tropospheric waves and moisture fluxes, since circulation diversity resulting from dissimilar locations and orientation are controlled for.

Two samples are selected to represent TTTs that occur in the two key zones of TTT activity shown in Fig. 3a: over the southern African continent and Madagascar. The samples were generated for each dataset by first restricting the event set to NDJFM and to the first day in each TTT event, then extracting TTTs with centroids



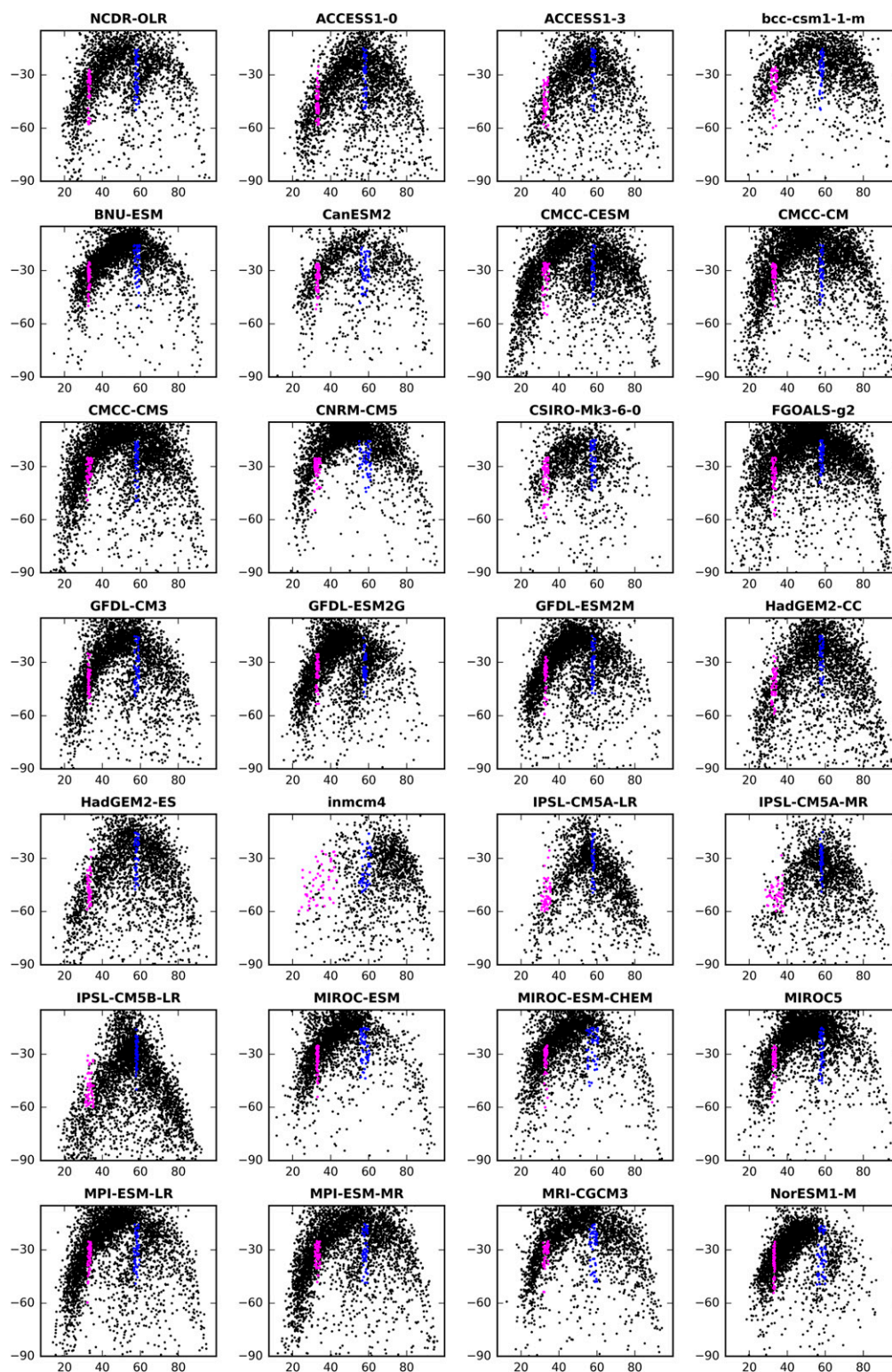


FIG. 4. Distribution of TTT centroid longitudes ( $x$  axis) and TTT orientations ( $y$  axis) in NCDR-OLR and 27 CMIP5 models. All NDJFM events are shown in black; samples are shown in pink (continental) and blue (Madagascar).

between 22° and 32°S. For the “continental” sample, the event set was then restricted to TTTs with angles of orientation between  $-60^\circ$  and  $-25^\circ$ , and finally the 50 TTTs with centroids closest to 33°E. For the “Madagascan” sample, TTTs with orientations between  $-50^\circ$  and  $-15^\circ$ , and closest to 58°E were selected. Figure 1 illustrates these features of the continental (pink) and Madagascan (blue) samples, and the TTTs selected to form the samples are shown in pink and blue on Fig. 4. This study focuses on the continental sample, since the continental TTT zone is more dominant (64% of observed TTTs occur west of 55°E) and contributes rainfall over southern Africa. Figure 5 shows a composite of the 50 sampled continental TTTs for each model and satellite data.

While the composites for each dataset (Fig. 5) do reveal some differences between satellite data and models, especially in terms of the OLR values over the Indian Ocean during continental TTT events, the composites are broadly consistent over subtropical southern Africa. The sampled TTTs are characterized by low OLR values extending from a region of tropical convection over the southern Congo Basin, southeast through Botswana, Zimbabwe, and eastern South Africa, over the southwest Indian Ocean, and into the Southern Ocean storm track. The cloud band is accompanied by areas of higher OLR values to the southwest and northeast, implying reduced cloud cover compared to the NDJFM daily average. It should be noted that the sampling has worked less well for INM-CM4, which simulates very few TTTs over southern Africa. For other models, the sample provides a good basis to evaluate circulation associated with southern African TTTs.

*b. Using the full event sets to analyze the frequency, location, and intensity of TTTs*

The full NDJFM event sets are used to compare the number, location, and intensity of TTTs between models. In Fig. 4, the distributions of TTT longitudes and angles of orientation reveal some features that are common across datasets. In NCDR-OLR (satellite data), the two zones of TTT activity identified in Fig. 3a are clear: with TTT centroids concentrated between 20°–40°E, over the southern African continent, corresponding to the continental (pink) sample, and between 55°–70°E, over Madagascar and the southwest Indian Ocean, corresponding to the Madagascan (blue) sample. The angle of orientation (shown on the y axis) varies between TTTs that are more meridional ( $< -60^\circ$  angle, toward the bottom of the y axis), and those that are more zonal ( $> -30^\circ$ , toward the top of the y axis). The more meridional TTTs ( $< -60^\circ$ ) are more likely to occur over the southern African continent: TTTs over Madagascar tend to have a more zonal orientation ( $> -50^\circ$ ). In each

of the two key zones (continental and Madagascan), TTTs that are farther east are more likely to have a more zonal orientation. This finding is in keeping with Fauchereau et al. (2009), who identify clusters of TTT days over the subcontinent, Mozambique Channel, and Madagascar, with clusters to the east having a more zonal orientation. This result suggests that as TTTs move eastward, or when they form farther east, their orientation is more zonal. TTTs east of 70°E are characterized by more meridional orientations, but this is likely an artifact of the domain used for extracting TTTs, which only extends to 100°E. These characteristics give the NCDR-OLR distribution in Fig. 4 a parabolic shape.

Many CMIP5 models capture this shape of the observed TTT distribution. However, it is immediately clear that some models (e.g., CMCC-CM) generate many more TTTs than others (e.g., CanESM2). There are also important differences in the proportion of events in the west or east of the domain. One notable outlier is INM-CM4, for which the majority of events occur to the east of Madagascar. This explains why the sampling technique in section 3a did not produce a very consistent composite for this model, further illustrated by the divergence in locations among the 50 TTTs designated as continental (in pink).

#### 4. Circulation associated with tropical temperate troughs

This section addresses the first research question: Do models simulate TTTs with similar circulation features to observed? TTTs are known to be accompanied by a ridge–trough–ridge structure, associated with an upper level wave in the midlatitudes (Todd and Washington 1999; Hart et al. 2010; Macron et al. 2014). They are also important sites of moisture convergence, and a south-eastward export of moisture from the tropics to the midlatitudes (Todd et al. 2004). Here we use the samples of 50 “continental” TTTs described in section 3a (Figs. 1 and 4) to examine these two circulation features, and to compare modeled circulation with an estimate of observed circulation. For each model, the sampled TTT dates are used to extract modeled  $u$ ,  $v$ ,  $\omega$ , and  $q$  data. To examine “observed” circulation, TTT dates from NCDR-OLR satellite data are used to select  $u$ ,  $v$ ,  $\omega$ , and  $q$  for the same dates from ERAI reanalysis.

Figure 6 shows composites of upper-level winds and vertical velocity to examine the wave structure associated with TTTs. Values are only shown for grid boxes where the 50-day composite is significantly different from all other NDJFM days, according to a Mann–Whitney  $U$  test. To avoid overinterpretation of multiple significance tests at gridpoint scale [as highlighted by Livezey and Chen (1983) and Wilks (2016)], false



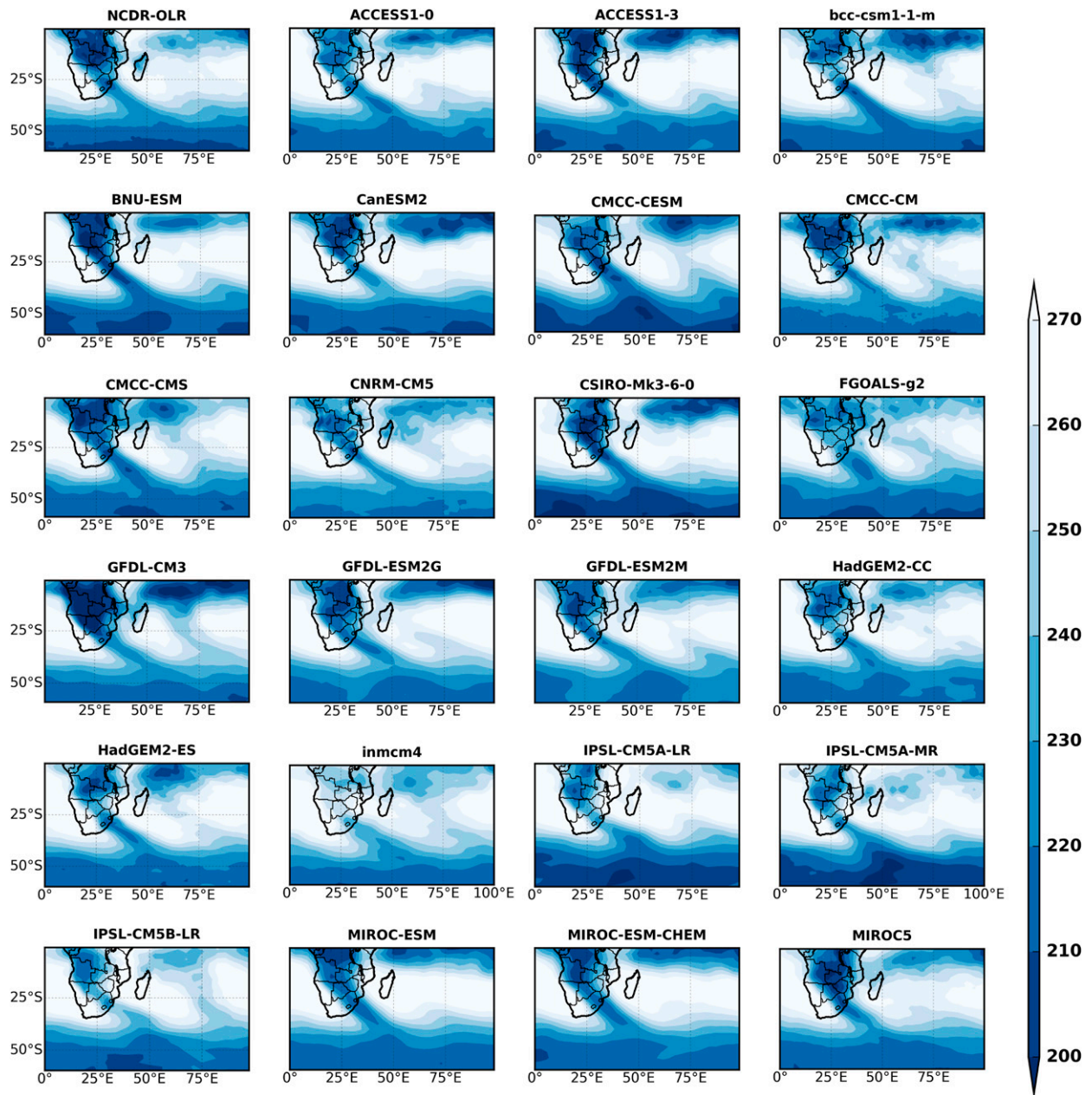


FIG. 5. Composites of mean OLR ( $\text{W m}^{-2}$ ) for 50 continental TTT days, sampled for satellite data (NCDR-OLR) and 27 CMIP5 models.

discovery rates (FDRs) are controlled using a  $p$  value ( $p_{\text{FDR}}^*$ ) calculated to be appropriate for the distribution of  $p$  values from all grid points, using a conservative significance level of  $\alpha_{\text{FDR}} = 0.05$ , following Wilks (2016).

The composites show a wave in the 250-hPa westerly winds extending from the midlatitudes into the subtropics, to approximately  $25^\circ\text{S}$ . This wave also manifests in  $\omega$  at 500 hPa, with uplift under the leading edge of the wave supporting the deep cloud of the TTT and



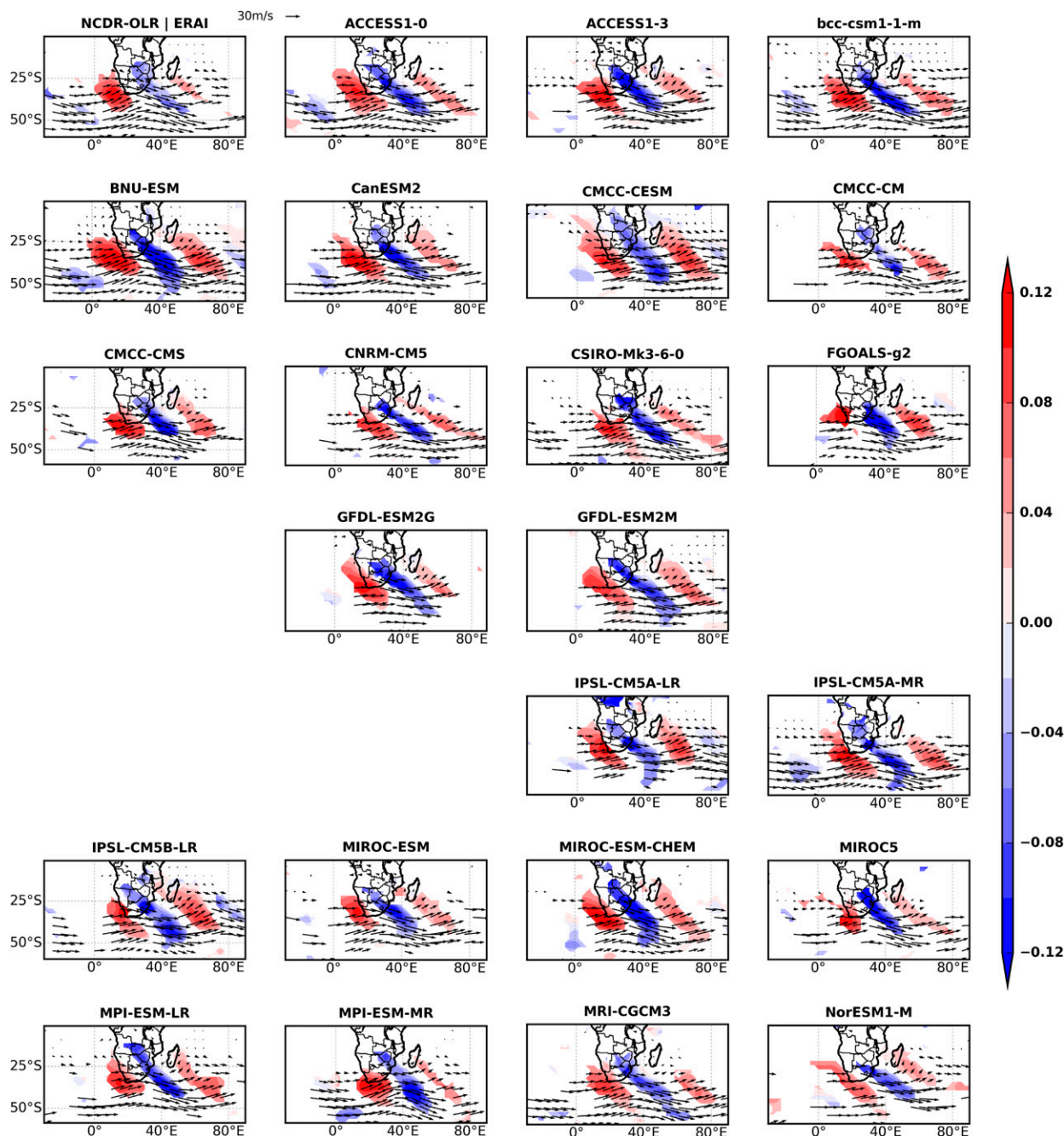


FIG. 6. Composites of mean 250-hPa wind (vectors;  $\text{m s}^{-1}$ ) and 500-hPa  $\omega$  (shading;  $\text{Pa s}^{-1}$ ) for the 50 continental TTT days sampled, for NOAA CDR (with circulation in ERAI) and each model with available data. A significance test is applied, and grid points where the composite is not significantly different from rest of time period are masked in white (controlling for FDR with  $\alpha_{\text{FDR}} 0.05$ ). For ease of visualization, all data are interpolated to a  $2.5^\circ \times 2.5^\circ$  grid.

subsidence to the northeast and southwest associated with ridges upstream and downstream of the trough. While there are differences in the extent and intensity of the wave in each composite, these features are qualitatively consistent among all of the models (Fig. 6). Analysis of lagged composites (not shown) reveals a

wave train over the South Atlantic two days prior to the TTT, which moves toward southern Africa at approximately  $5^\circ$  longitude per day. This is consistent with prevailing understanding that TTTs form as westerly waves propagate northeastwards from the midlatitudes into a region of negative zonal stretching deformation

over southern Africa and the adjacent Indian Ocean (Widlansky et al. 2011; Vignaud et al. 2012; Macron et al. 2014).

Figure 7 shows composites of moisture flux (vectors:  $qu$ ,  $qv$ ) and  $q$  at 850 hPa, to examine the water vapor transport associated with TTTs in models and reanalysis. As in Fig. 6, values are only shown where the composite is significantly different from other NDJFM days. Anomalous high humidity and poleward moisture flux is clear in the region of the cloud band, extending beyond 45°S in most models. Some models also show regions of anomalously low moisture to the northeast and southwest of the TTT, corresponding to the ridges shown in Fig. 6. There are notable differences between models in the magnitude of anomalous specific humidity, suggesting systematic model differences in the intensity of moisture convergence in simulated TTTs. There is thus important intermodel variation, but the southeastward export of moisture is consistently shown.

The analysis of 50 commonly located TTTs in each dataset therefore illustrates that all models analyzed generate TTTs over the southern African continent with circulation features that are qualitatively similar to those observed, including a ridge–trough–ridge structure, and southeastward moisture export. The same conclusion was reached for analysis (not shown) of 50 TTTs over Madagascar (blue dots in Fig. 4).

## 5. Frequency, location, and intensity of tropical temperate troughs

While modeled TTTs have similar structures to those observed, there are important differences between models in the frequency and location of events (Fig. 4), and possibly their intensity (Fig. 7). This raises the second research question: How do the number, location, and intensity of TTTs compare between models? Also, how do these characteristics relate to precipitation biases? CMIP5 models have been found to exhibit a large range in the amount of summer precipitation over southern Africa, with the majority of models showing wet biases (Munday and Washington 2017). Since TTTs contribute an important proportion of summer rainfall (Harrison 1984; Washington and Todd 1999; Hart et al. 2013), it is worth investigating whether model representation of TTTs can explain why models are often too wet over southern Africa, or why some models are much wetter than others.

### a. Metrics of frequency, location, intensity, and precipitation biases

Three metrics have been computed to represent the frequency, location, and intensity of TTTs (Figs. 8a–c).

To examine frequency (Fig. 8a), we calculate the total number of NDJFM TTTs averaged over 35 years, to give an indication of the models' general tendency to generate more or fewer TTTs in the SICZ region. However, it is clear from Fig. 4, and previous analysis of the Met Office Unified Model (James et al. 2018), that models differ in their preferred location of TTTs within the SICZ. For example, HadGEM3-GC2 was found to produce many events over the Indian Ocean (James et al. 2018). To quantify the preferred longitudinal location for TTTs in each model (Fig. 8b), the percentage of TTTs with centroids west of 55°E is calculated. We have found that TTTs extending from Madagascar, in the eastern TTT zone shown in Fig. 3a, are well characterized by sampling centroids closest to 58°E (blue star in Fig. 1). Therefore our metric, centroids west of 55°E (orange line in Fig. 1), is a proxy for the proportion of TTTs over the southern African continent and Mozambique Channel, versus TTTs over Madagascar and farther east in the western Indian Ocean. In short, it quantifies the proportion of TTTs that are “continental.” The third metric, for intensity of TTTs (Fig. 8c), is designed to measure the rainfall contributed by TTTs in different models. Since we are primarily interested in rainfall over southern Africa, we quantify the average rainfall per TTT day over subtropical southern Africa (15°–40°E, 20°–35°S; blue shaded box in Fig. 1).

Each of the three metrics is related to precipitation biases in Figs. 8a–c, with 1) frequency, 2) location, and 3) intensity on the  $x$  axes, and precipitation biases on the  $y$  axes. In Fig. 8a, the precipitation biases are computed over a large subtropical domain extending over southern Africa and the Indian Ocean (7.5°–100°E, 20°–35°S; gray shaded box in Fig. 1), since the frequency metric is based on the full SICZ TTT count. In Figs. 8b and 8c precipitation biases are computed for subtropical southern Africa (15°–40°E, 20°–35°S; blue shaded box in Fig. 1), as these metrics quantify the proportion and intensity of continental TTTs.

The frequency of TTTs (Fig. 8a) varies markedly between models. In satellite data (in pink), 74 TTTs are detected per year. In contrast, INM-CM4 and CanESM2 generate <40 events per year, while FGOALS-g2 generates >140, almost double the number observed. TTTs occur on 49% of NDJFM days in NCDR-OLR, and almost 94% of days in FGOALS-g2. It is important to establish that this is a genuine distinction in the modeled weather, rather than an artifact of applying the software to models with different mean climates. As noted in section 3, the cloud band identification process relies on, and is sensitive to, a threshold for low OLR values. With a lower threshold, fewer events are detected and with a higher threshold more events are

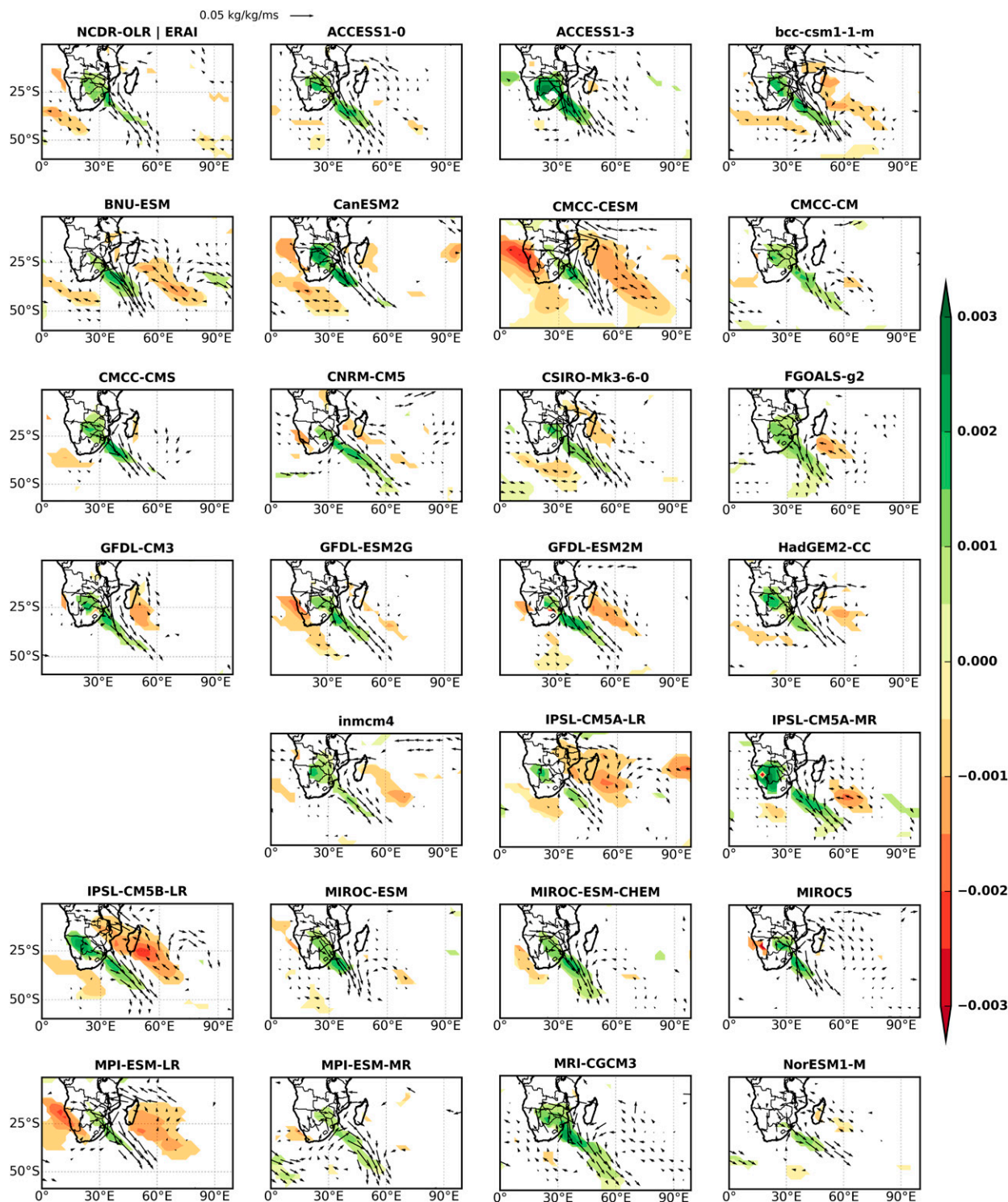


FIG. 7. Composites of mean 850-hPa qflux (vectors;  $\text{kg kg}^{-1} \text{m s}^{-1}$ ) and specific humidity (shading;  $\text{kg kg}^{-1}$ ) for the 50 continental TTT days sampled, as an anomaly from the long-term NDJFM mean, for NOAA CDR (with circulation in ERAI) and each model with available data. Significance testing and interpolation follow the same procedure as Fig. 6.



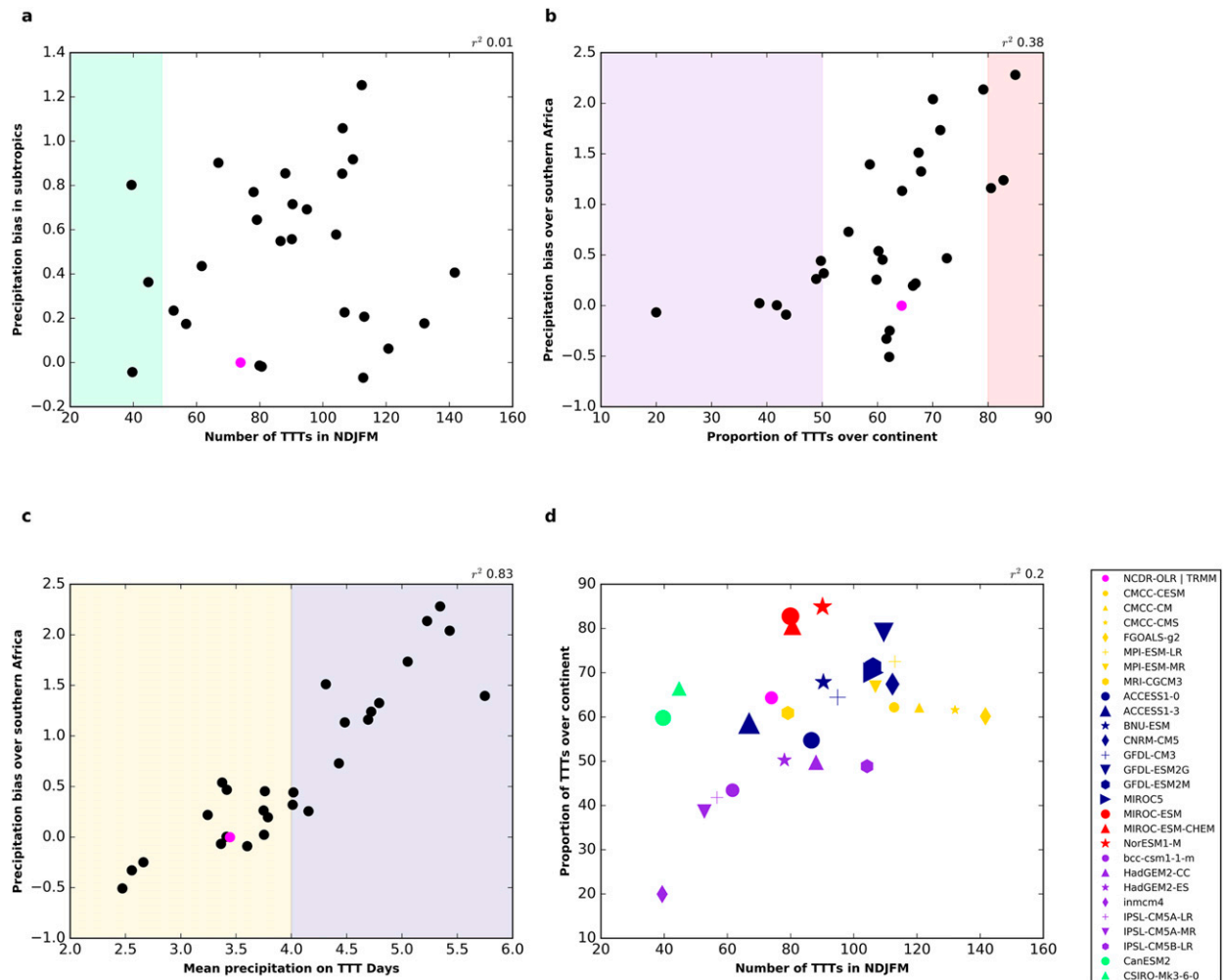


FIG. 8. Distribution of TTT characteristics across models, and relationship with precipitation biases: (a) Number of TTTs per year against precipitation biases over the subtropical domain ( $7.5^{\circ}$ – $100^{\circ}$ E,  $20^{\circ}$ – $35^{\circ}$ S), (b) proportion of continental TTTs (with centroids west of  $55^{\circ}$ E) against precipitation biases over subtropical southern Africa ( $15^{\circ}$ – $40^{\circ}$ E,  $20^{\circ}$ – $35^{\circ}$ S), and (c) intensity of precipitation on TTT days (based on average precipitation over subtropical southern Africa), against precipitation biases as in (b). (d) The number of TTTs [as in (a);  $x$  axis], proportion of continental TTTs [as in (b);  $y$  axis], and intensity of TTT precipitation [as in (c); shown by the size of the dot]. In (a)–(c), TTT characteristics are shown on the  $x$  axis and precipitation biases on the  $y$  axis, with each CMIP5 model a black circle, and satellite data a pink circle. In (d), these three TTT characteristics are replotted together, and models are color-coded to represent their “group” (as described in Fig. 9 and Table 2), illustrating how models can be categorized according to their TTT characteristics. The grouping criteria are also shaded in (a)–(c). All data are for NDJFM, and all precipitation biases are relative to TRMM in  $\text{mm day}^{-1}$ .

detected. Figure 8 was recomputed with higher and lower OLR thresholds, revealing that the values for each dataset/model are sensitive to changes in the threshold, but the relationship across models is not (see Figs. S1 and S2). If the threshold is lowered or raised, the number of events in all models changes consistently, which maintains the intermodel relationships. With a lower OLR threshold, FGOALS-g2 has fewer TTTs detected, but still more than any other model, and approximately double the number observed in satellite data. This confirms that there is a genuine difference between modeled TTT frequencies, and it is not an artifact of the

cloud band sampling methodology. This stark difference in the number of TTTs cannot explain the variation in rainfall over the subtropical domain (Fig. 8a). Some of those models with the largest TTT frequencies have little or no wet bias, and some models that overestimate rainfall have fewer TTTs than observed. This finding holds when the analysis is repeated for continental TTTs only (not shown).

The preferred location of TTTs appears to have more explanatory power over model variation in rainfall over southern Africa (Fig. 8b). It has already been noted (Fig. 4) that INM-CM4 generates few TTTs over continental southern Africa, and more over the Indian



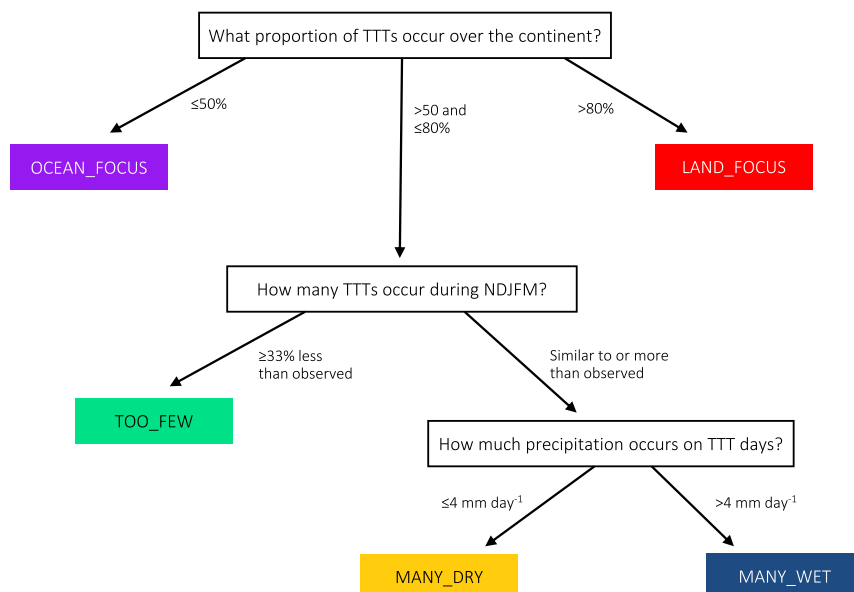


FIG. 9. Flowchart to illustrate algorithm for grouping models.

Ocean. Figure 7b shows that <20% of TTTs in INM-CM4 occur over the continent. This is in contrast to the satellite estimate that 64% of TTTs are continental. In three models >80% of TTTs occur west of 55°E. These differences in location explain 38% of variation in continental precipitation biases ( $r^2 = 0.38$ ): models that focus TTTs over the continent tend to produce more rainfall there, and models that have a greater proportion of TTTs over Madagascar and the Indian Ocean have less rainfall over the southern African subcontinent.

The intensity of TTTs is also associated with the variation between models in precipitation over this southern African domain ( $r^2 = 0.83$ ). While in satellite data TTT days produce an average of 3.4 mm day<sup>-1</sup>, in models this number ranges from 2.5 to 5.8 mm day<sup>-1</sup>. Those models that contribute more rain per TTT day also have the largest mean precipitation biases, and vice versa.

Figures 8a–c therefore demonstrate large discrepancies between models, in the number of TTTs, the preferred longitudinal location of TTTs, and the amount of precipitation associated with TTTs. While the frequency of SICZ TTTs does not explain intermodel differences in subtropical precipitation, the preferred location and intensity of TTTs are associated with intermodel variability in continental precipitation biases. These findings suggest that there is no straightforward relationship between TTTs and rainfall across models. Rather, different models exhibit different TTT behaviors and tendencies, raising the possibility that models might be grouped according to their TTT characteristics. Grouping models has potential to help describe and aid

understanding of differences between TTT climatologies. By identifying intragroup commonalities and intergroup differences, we can determine the processes and features which relate to TTT activity, and therefore highlight focus areas for model development to improve representation of TTTs. Grouping models might also help to interpret and assess divergence in models' future projections.

#### b. Grouping models by TTT characteristics

The three metrics for frequency, location, and intensity are used to group CMIP5 models according to their TTT behavior. The grouping algorithm is illustrated in Fig. 9, and functions as follows. First, the proportion of TTTs west of 55°E is used to identify models that have a "LAND\_FOCUS" or "OCEAN\_FOCUS" in TTTs. The second stage of the grouping process is based on the number of NDJFM TTTs per year. Those models with at least a third less than observed are placed into the "TOO\_FEW" group. Finally, the intensity is used to distinguish between the "MANY\_DRY" group, which have many TTTs but with limited precipitation per TTT day, and the "MANY\_WET" group, which have >4 mm of precipitation per TTT day. The grouping criteria are also shaded in Figs. 8a–c, and more information about each group is provided in Table 2.

There are elements of the grouping algorithm that are subjective: the order of the steps in Fig. 9, and the thresholds that distinguish between groups. There are several models that, with a slight change to the algorithm, would fall into a different group. Notably, INM-CM4, which is in the OCEAN\_FOCUS group, could also fit within the TOO\_FEW group, with only 39 TTTs

TABLE 2. TTT characteristics of model groups. Distinguishing criteria are shown in bold.

Group	Number of TTTs per NDJFM	Proportion of TTTs over continent	Mean precipitation on TTT days ( $\text{mm day}^{-1}$ )	Members
<b>Observations</b>	74	64%	3.4	NCDR-OLR
<b>OCEAN_FOCUS</b> TTTs focused over ocean	39–104	20%–50% <b>Criterion <math>\leq 50\%</math></b>	3.4–4.0	BCC-CSM1.1-m HadGEM2-CC HadGEM2-ES INM-CM4 IPSL-CM5A-LR IPSL-CM5A-MR IPSL-CM5B-LR
<b>LAND_FOCUS</b> TTTs focused over continent	80–90	81%–85% <b>Criterion <math>&gt; 80\%</math></b>	4.7–5.3	MIROC-ESM MIROC-ESM-CHEM NorESM1-M
<b>TOO_FEW</b> Few TTTs	40–45 <b>Criterion: <math>\geq 33\%</math> less than observed</b>	60%–66%	3.8–4.2	CanESM2 CSIRO-Mk3.6.0
<b>MANY_DRY</b> Many TTTs but limited rain per event	79–142	60%–73%	2.5–3.8 <b>Criterion: <math>\leq 4</math></b>	CMCC-CESM CMCC-CM CMCC-CMS FGOALS-g2 MPI-ESM-LR MPI-ESM-HR MRI-CGCM3
<b>MANY_WET</b> Many TTTs, lots of rain per event	67–112	55%–79%	4.3–5.8 <b>Criterion: <math>&gt; 4</math></b>	ACCESS1.0 ACCESS1.3 BNU-ESM CNRM-CM5 GFDL-CM3 GFDL-ESM2G GFDL-ESM2M MIROC5

per NDJFM season. It is also worth noting that, due to the small size of the groups, it is not possible to test the differences between them statistically. These facts do not undermine the purpose of the grouping, which is not to establish quantitative or statistical significance between models or model groups, but to develop a more in-depth understanding of the processes that relate to TTT activity.

The result of the grouping is shown in Fig. 8d, where the three indices are replotted on the same axes (frequency on the  $x$  axis, location on the  $y$  axis, intensity as size of dot), and different colors represent each group. The groups clearly occupy different areas of this plot. The  $y$  axis (location) clearly divides the red LAND\_FOCUS models, which concentrate TTTs over the continent and have higher continental precipitation, and the purple OCEAN\_FOCUS models, which have more TTTs over the Indian Ocean. The other models, without a strong longitudinal bias in TTTs, sit between these groups, and are distinguished by the  $x$  axis, which highlights the green TOO\_FEW group, and the size of

the dot, which marks the difference between the smaller, yellow MANY\_DRY models, which have lots of TTTs but with limited rainfall, and the larger, navy MANY\_WET models, which have more rainfall per TTT.

## 6. Diagnosing intermodel differences

Having identified important distinctions between models and satellite data, and five different types of modeled TTT behavior, in this section we address the third research question: What factors are associated with intermodel differences in the number, frequency, and intensity of TTTs? Given the nature of the CMIP5 “ensemble of opportunity” in which each model’s structure and parameterization differs from the next in myriad ways (Knutti et al. 2010), it is not possible to definitively establish the causes of divergence in emergent behavior. However, careful diagnosis of intermodel differences can provide useful insights for model development and further research.

### a. Tropical convection

TTTs result from an interaction between tropical convection and extratropical waves and are often preceded by convective activity over tropical southern Africa (Macron et al. 2014). CMIP5 models are known to have marked contrasts in the amount of precipitation in the Congo Basin (Creese and Washington 2016) and important divergence in the modeled Indian Ocean Walker circulation (Hirons and Turner 2018), findings that suggest potential for strong variation between models in the amount and location of simulated convective activity. Modeled variation in climatological convective activity might therefore help diagnose contrasts in TTT behavior.

Figure 10 reveals large differences between models and satellite data in the spatial distribution of mean NDJFM OLR. It is worth noting that subtropical OLR has substantial intermodel variability, as would be expected from the intermodel variability in TTT frequency. We find a strong correlation ( $r^2 = 0.6$ ) between domain-averaged subtropical OLR and number of TTTs across the CMIP5 ensemble. For example FGOALS-g2 has relatively low OLR in the subtropics compared to satellite data, and this model has a TTT detected on 94% of NDJFM days. While this OLR–TTT relationship is expected, the result diagnoses that some models may have more suitable conditions for convective instability in the subtropics in general. Likewise, it may be that subtropical convection is inhibited in models with high subtropical OLR and few TTTs [such as the TOO\_FEW (green) models].

In the tropics, Fig. 10 also indicates clear intermodel differences. Observed OLR shows marked zonal asymmetry which maps on to the Walker circulation: the lowest OLR values are over the Congo Basin linked to upward mass flux, and higher OLR values in East Africa and the west equatorial Indian Ocean, where subsidence inhibits convection. Many models do not reproduce this asymmetry, with low OLR values extending zonally across west equatorial Indian Ocean. There is also substantial intermodel divergence in the magnitude of low OLR over the Congo convective region. This is further illustrated by Fig. 11, which displays tropical mean OLR at a range of longitudes over the African continent and Indian Ocean (purple shaded region in Fig. 1). This figure is based on December to February (DJF), rather than the full NDJFM TTT season, to focus on the peak location of convective activity during austral summer.

We investigate whether convective activity in the Congo Basin relates to the number of TTTs over southern Africa, by plotting mean OLR in the south of the Congo Basin (green shaded box in Fig. 1) against the number of

continental TTTs (Fig. 12a), again focusing on the peak summer season (DJF). We find that the amount of convective activity in the Congo Basin can statistically explain 37% of the intermodel variation in number of continental TTTs.

It is also possible that the common model tendency to show low OLR values in the western Indian Ocean, approximately 50°–80°E (Figs. 10 and 11), indicating tropical convective activity in what should be a subsidence region, could be associated with TTT formation over the Indian Ocean. In section 5 we found large variation between models in the longitudinal location of TTT activity. This is further illustrated by Fig. 13, which shows the spatial distribution of TTTs in satellite data (as in Fig. 3a) and each model. Note the contrast between LAND\_FOCUS (red) models, which predominantly generate TTTs over the continent or Mozambique Channel, and OCEAN\_FOCUS (purple) models, which have at least half of their TTTs west of 55°E. While some models in the OCEAN\_FOCUS (purple) group focus TTT activity in the Madagascan region, where many TTTs are observed in satellite data, others, such as BCC-CSM1.1-m, focus TTTs even farther east than Madagascar, where very few TTTs occur in nature, indicating a clear divergence from reality. Figure 11 shows that the OCEAN\_FOCUS models (purple) underestimate deep convection over central Africa, and most overestimate convection over the ocean between 50°–80°E, as shown by the OLR values well below those observed. In contrast, the LAND\_FOCUS (red) models have more convective activity over the Congo Basin, and in the case of NorESM1-M, more than observed. Figure 12b, shows that OLR values in the southern Congo Basin (green shaded box in Fig. 1) are strongly correlated with the proportion of TTTs over the continent ( $r^2 = 0.63$ ). Therefore, it appears that models with more convection in the Congo Basin are more likely to focus TTTs over the continent, whereas models with weaker Congo Basin convection (and relatively high convective activity in the western Indian Ocean) are more likely to focus TTTs farther east over the Indian Ocean.

### b. Subtropical moisture supply

Subtropical moisture supply is another factor that might help diagnose variation in modeled TTT behavior. Influx of moisture is crucial to supporting the moist convective environments necessary for TTT development (e.g., Hart et al. 2018a). Previous work has shown intermodel variation in moisture flux into southern Africa. In particular, Munday and Washington (2018, hereafter MW18) have recently highlighted the importance of the northeast monsoon, finding a strong relationship between northeasterly moisture flux into southern Africa and intermodel variation in southern African summer

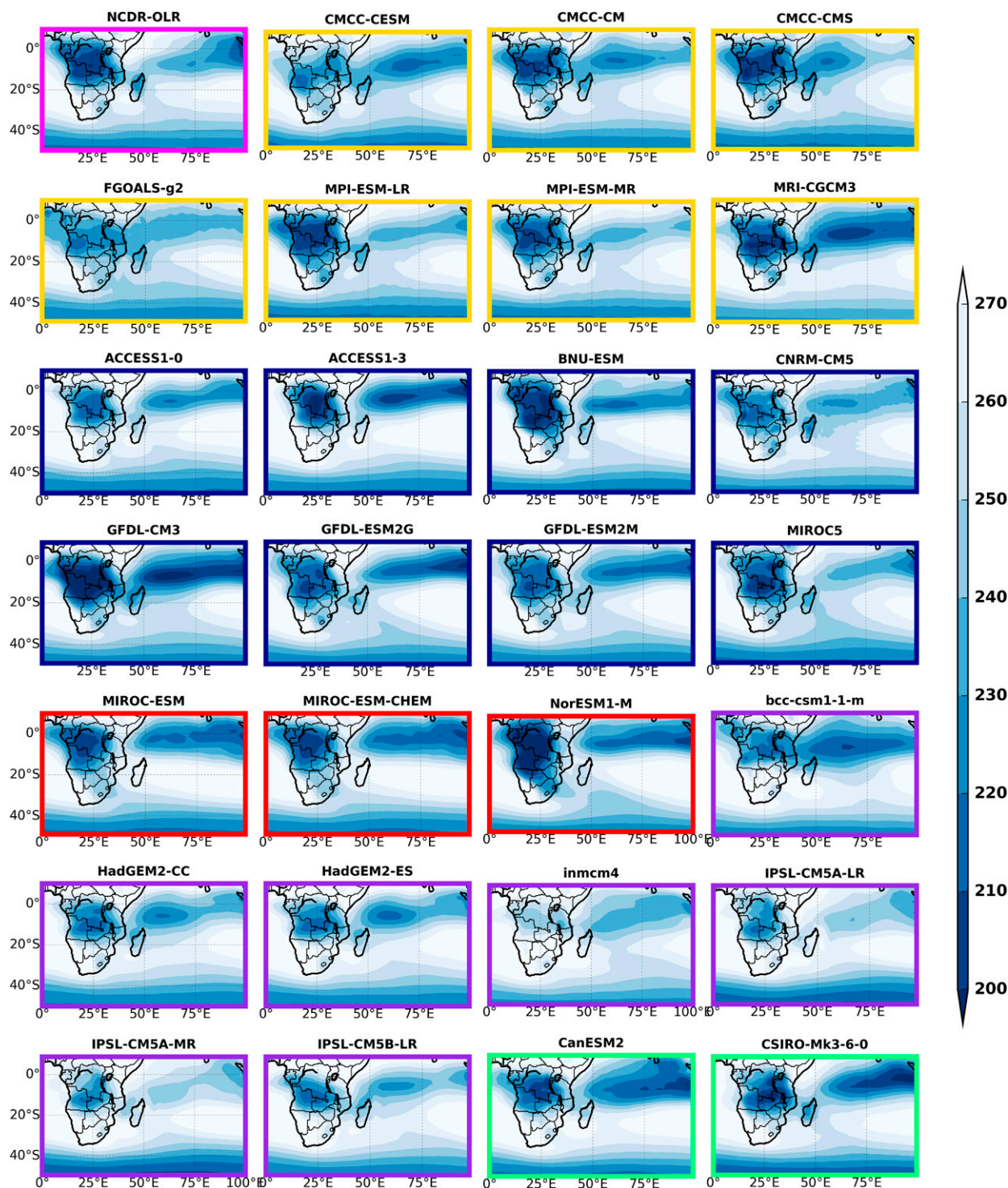


FIG. 10. Mean NDJFM OLR ( $\text{W m}^{-2}$ ) in satellite data and 27 models. The border of each plot indicates the model group (see Table 2).

precipitation. Figure 14 shows climatological moisture fluxes at 850 hPa in ERAI during DJF, when the northeast monsoon is active. In nature, part of the northeasterly flow into the subcontinent is blocked by topography, and re-circulates in an anticlockwise direction toward Madagascar.

In many models, the moisture flow into southern Africa is overestimated, associated with the reduced height of the Tanzanian Escarpment and/or higher wind speed upstream of this feature (MW18). As a consequence, MW18 have argued, such models produce too much



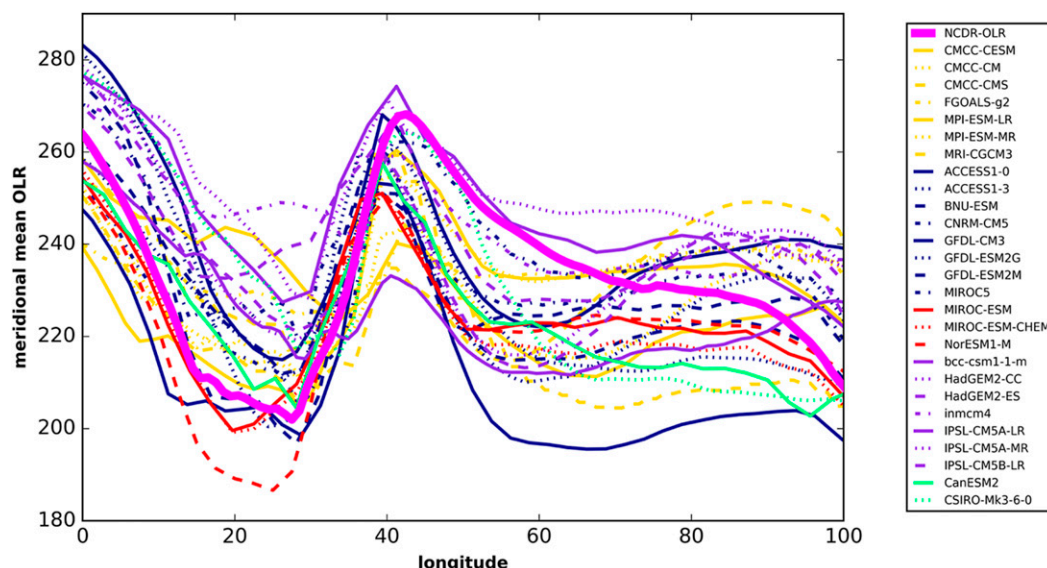


FIG. 11. Mean DJF equatorial OLR ( $0^{\circ}$ – $10^{\circ}$ S) ( $\text{W m}^{-2}$ ) at each longitude, in satellite data and 27 models. Colors show the group to which each model has been assigned, as defined in Table 2.

rainfall over southern Africa, and often underestimate rainfall over Madagascar (as little moisture flux is diverted to the southeast). Several of these models highlighted by MW18 are in our LAND\_FOCUS (red) group, including the MIROC-ESMs.

Here we investigate whether the magnitude of the northeasterly moisture flux in models is related to TTT activity. We apply the index developed by MW18 based on the nondimensional Froude number ( $F_n$ ) to give a measure of the ability of the northeasterly flow to pass

over the Tanzanian Escarpment. Their index is based on January to February (JF), when the northeasterly flow is most stable (during December more zonal, easterly, flow can dominate). Based on the mean wind velocity at  $36^{\circ}$ – $42^{\circ}\text{E}$ ,  $3^{\circ}$ – $11^{\circ}\text{S}$  (dark green outline in Fig. 1), the buoyancy frequency, and the height of model Tanzanian topography,  $F_n$  is small if the flow is blocked substantially by the topography, and large if there is limited restriction from topography on the wind flow. Figure 15 shows that climatological  $F_n$  statistically

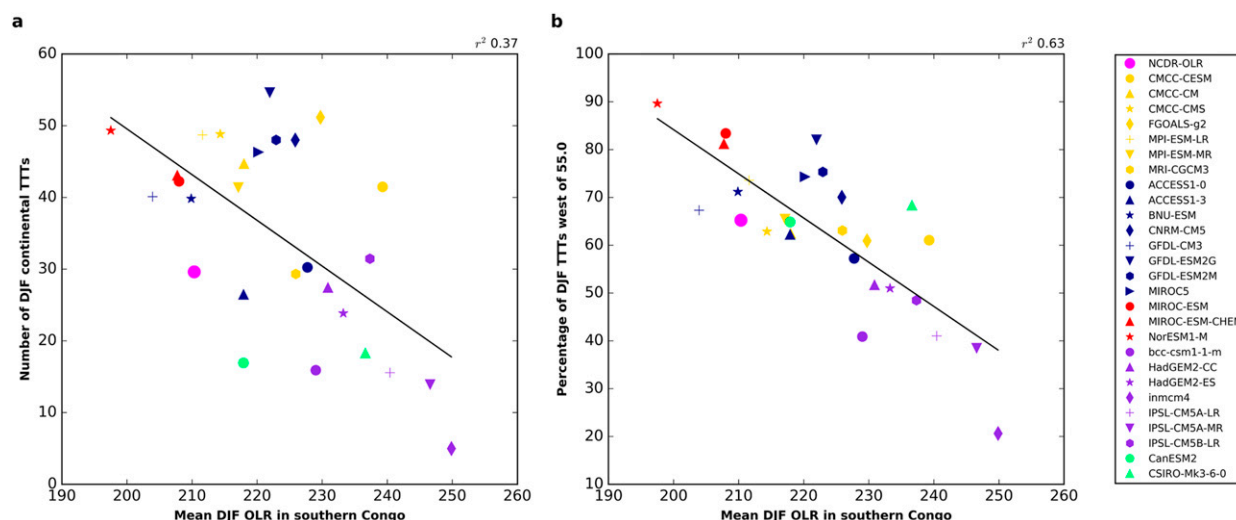


FIG. 12. Relationship between mean DJF OLR in the south of the Congo Basin ( $7.5^{\circ}$ – $100^{\circ}\text{E}$ ,  $20^{\circ}$ – $35^{\circ}\text{S}$ ) ( $\text{W m}^{-2}$ ) and TTT activity: (a) number of DJF TTTs over the continent (east of  $55^{\circ}\text{E}$ ) and (b) percentage of DJF TTTs west of  $55^{\circ}\text{E}$ . Colors indicate model groups (see Table 2). The coefficient of determination ( $r^2$ ) is displayed to the top right of each plot.

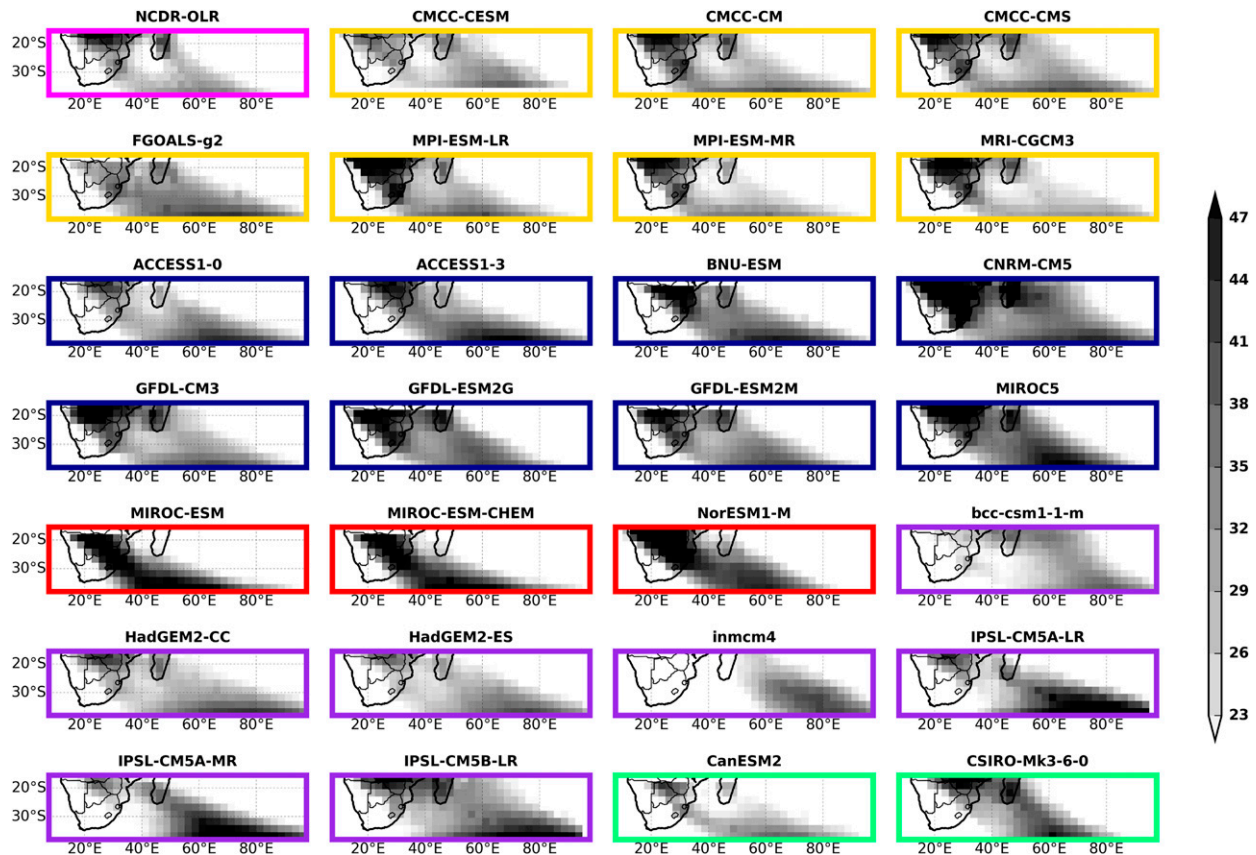


FIG. 13. Spatial distribution of NDJFM TTTs in satellite data and 27 models, based on the percentage of TTT days when a TTT cloud band covers each box in a  $2.5^\circ \times 2.5^\circ$  grid. The border of each plot indicates the model group (see Table 2).

explains 48% of the intermodel variation in the proportion of TTTs over the continent (Fig. 15a), and 44% of the variation in the intensity of TTTs (Fig. 15b). Models with higher  $F_n$  (i.e., less blocking and therefore more northeasterly flow into southern Africa) have a higher proportion of TTTs over the continent, and more precipitation per continental TTT. Anomaly maps of moisture flux (Fig. 14) further illustrate the enhancement of the northeasterly flow in the LAND\_FOCUS models. In the LAND\_FOCUS composite climatology (not shown) there is no northwesterly flow toward Madagascar. In contrast, the OCEAN\_FOCUS models have anomalously strong northwesterly monsoonal flow toward Madagascar.

Topography appears to be one of the drivers of divergence between models. Differences in the modeled height of the Tanzanian Escarpment in CMIP5 are large (MW18), as are differences in orography over Madagascar. Barimalala et al. (2018) have recently demonstrated the importance of Madagascar orography for southern African rainfall by progressively flattening and then removing Madagascar in idealized experiments. As they show, Madagascar orography strongly influences the strength of the northwesterly recurvature. In keeping with this,

models in the LAND\_FOCUS (red) group, which have no northwesterly flow, dramatically underestimate the height of Madagascar. MIROC-ESM models have a mean height of Madagascar orography ( $11^\circ$ – $26^\circ$ S,  $42^\circ$ – $51^\circ$ E) less than 100 m, compared to averaged height over 600 m in GTOP030.

Another feature associated with the modulation of moisture transport into the subcontinent is the Angola low (Mulenga et al. 2003; Cook et al. 2004; Rouault et al. 2003; Howard and Washington 2018). This feature is thought to influence the influx of moisture from the southeastern Atlantic and western Indian Oceans. Differences in the latitude and strength of the Angola low have been found to be associated with rainfall magnitude and location in southern Africa (Cr  tat et al. 2018). Munday and Washington (2017) showed that there is large variation between CMIP5 models in the mean strength of the DJF Angola low, and this variation correlates closely with modeled precipitation over southern Africa, particularly Zambia and southern Mozambique.

Here we apply the Angola low index developed by Munday and Washington (2017), and examine the relationship with continental TTT intensity (Fig. 15c),

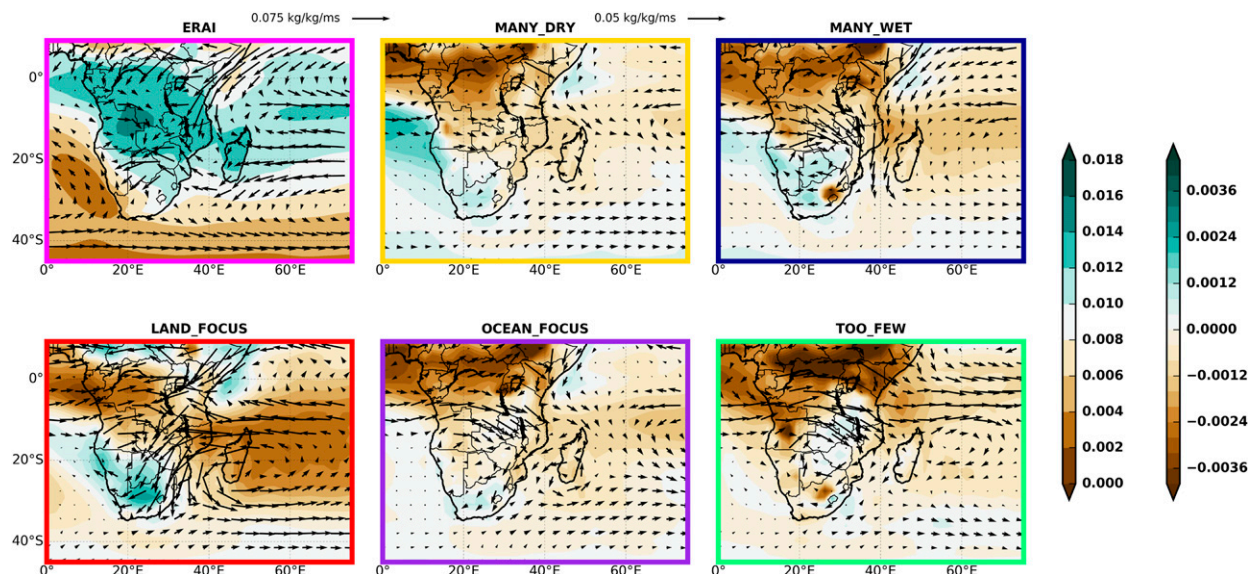


FIG. 14. Moisture flux (vectors;  $\text{kg kg}^{-1} \text{m s}^{-1}$ ) and specific humidity (contours;  $\text{kg kg}^{-1}$ ) at 850 hPa in DJF, in ERAI reanalysis (climatological mean; left color bar), and a composite of each model group, as an anomaly from the ERAI mean (right color bar). To aid visualization, all data are interpolated to a  $1.75^\circ \times 1.75^\circ$  grid.

focusing on DJF, when the Angola low is dynamically a tropical low. The index is based on the mean geopotential height with the lowest 5% of DJF mean 850-hPa geopotential height values within a large southern African domain ( $5^\circ\text{--}55^\circ\text{E}$ ,  $0^\circ\text{--}35^\circ\text{S}$ ). The figure suggests that models with more intense continental TTTs (MANY\_WET models; in navy) have a stronger mean Angola low than models with less rainfall per TTT (MANY\_DRY models; in yellow). While the  $r^2$  value suggest that the Angola low only accounts for 29% of the variance in TTT intensity, this includes the OCEAN\_FOCUS models, which have a strong mean

Angola low but medium TTT intensity over the continent, partly related to the weaker northeasterly inflow. If the OCEAN\_FOCUS models are removed, the  $r^2$  value is 0.7. The strength of the Angola low thus is a useful diagnostic of TTT intensity for models simulating many TTTs over southern Africa.

### c. Upper-level westerly flow

TTTs form when tropical convection and subtropical moist environments, discussed above, interact with upper-level westerly wave disturbances propagating into the region (Harrison 1984; Taljaard 1996) as shown in Fig. 6.

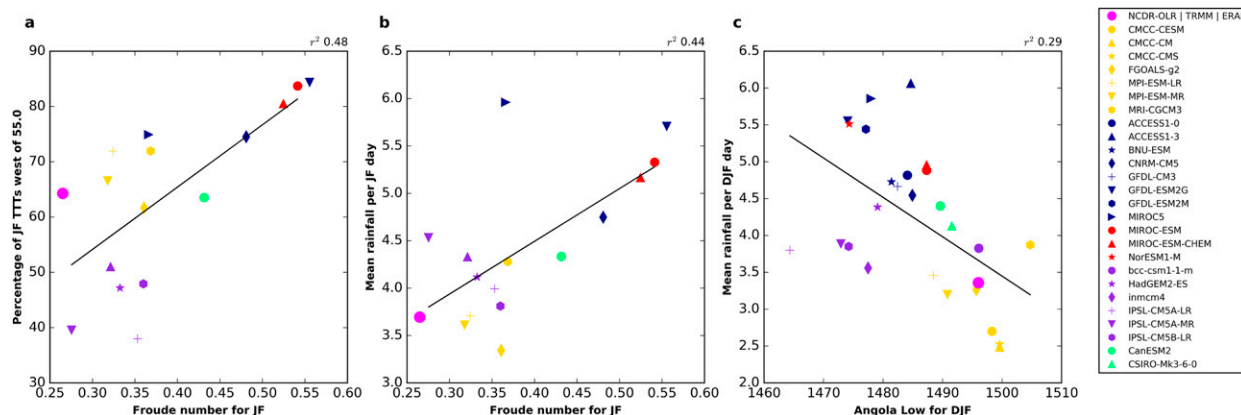


FIG. 15. Relationship between Froude number (following MW18) and (a) percentage of JF TTTs west of  $55^\circ\text{E}$  and (b) average rainfall per TTT day (mm) over subtropical southern Africa ( $15^\circ\text{--}40^\circ\text{E}$ ,  $20^\circ\text{--}35^\circ\text{S}$ ) in JF. (c) Relationship between mean strength of the Angola low [following Munday and Washington (2017)] and average rainfall per TTT day (mm) over subtropical southern Africa ( $15^\circ\text{--}40^\circ\text{E}$ ,  $20^\circ\text{--}35^\circ\text{S}$ ) in DJF. Colors indicate model groups (see Table 2).



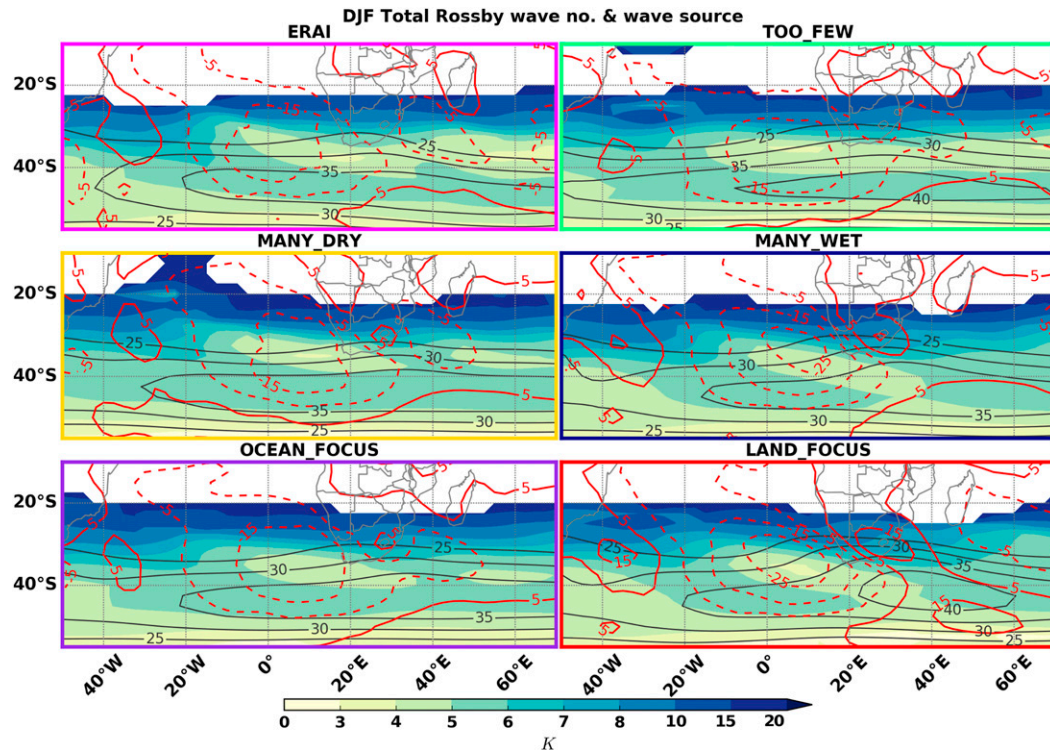


FIG. 16. Rossby wave diagnostics for 200-hPa DJF mean flow in reanalysis (ERA1) and CMIP5 model groupings (see Fig. 9). Total Rossby wavenumber  $K$  for wave phase speed  $c = 6 \text{ m s}^{-1}$  (shading;  $K > 25$  or  $U_{\text{mean}} - c < 0$  is masked out) is overlaid by mean zonal wind (gray contours) and Rossby wave source (positive values in solid red contours, dashed for negative values).

Rossby wave theory, considered using 200-hPa mean wind, provides a useful framework for diagnosing the implications of model mean state differences on wave propagation in the region. Here we compute the total Rossby wavenumber  $K$  (Hoskins and Karoly 1981; Hoskins and Ambrizzi 1993) and the Rossby wave source (RWS; Sardeshmukh and Hoskins 1988). We compute  $K$  for waves with phase speed  $c$  of  $6 \text{ m s}^{-1}$  [as in van der Wiel et al. (2015)], which is appropriate for the synoptic waves of relevance to TTTs. This analysis extends results in Hart et al. (2018a,b) which demonstrate the association between local subtropical jets, meridional shear, and TTT activity. Meridional shear ( $d\bar{u}/dy$ ), the meridional component of relative vorticity, is a key term in the computation of both  $K$  and RWS.

Figure 16 presents the DJF ERA1 climatology of these diagnostics alongside composites for each model grouping. Each of the CMIP5 groupings capture the gross features of this sector of the Southern Hemisphere with the spatial patterns of the westerly jet at 200 hPa,  $K$ , and RWS all broadly correct. However, there are important differences between groups. An overly strong midlatitude jet is associated with the TOO\_FEW group, similar to El Niño seasons in the observed climate, when there is an anomalously strong eddy-driven jet and are

fewer cloud bands (Lindesay 1988; Hart et al. 2018b). The strong jet supports a distinct waveguide across the Atlantic–Indian sector. This extratropical waveguide, supporting wavenumbers 5–6, is separated from the subtropics by zonal corridor of lower wavenumbers. The resultant zonal propagation over waves along the waveguide would be unfavorable for TTT formation.

The MANY\_DRY and OCEAN\_FOCUS composites are very similar to ERA1 (Fig. 16). The midlatitude jet is weaker than in the TOO\_FEW composite, which diminishes the separation of the waveguide from the subtropics. This flow would support more propagation of waves from the midlatitudes into the subtropics. Subtropical gradients in  $K$  control the equatorward refraction of Rossby waves (Hoskins and Ambrizzi 1993; van der Wiel et al. 2015) and as seen from observations (Fig. 2a) and the ERA1 flow here, TTTs form across a wide range of longitudes in the SICZ. However, the weaker  $K$  gradients in the OCEAN\_FOCUS composite mean waves likely undergo weaker equatorward refraction and therefore trigger TTTs farther east in the SICZ.

A substantial zonal asymmetry bias is diagnosed for the MANY\_WET and LAND\_FOCUS groupings. Modified gradients of  $K$  could favor more equatorward refraction of waves over the subcontinent (Fig. 16). This



asymmetry may in part be forced by more intense deep convection in the Congo (as noted earlier; Fig. 12). However, it is also likely self-reinforcing, as indicated by the notable Rossby wave source values over the continent. Frequent TTTs support intense off-equatorial deep convection with the cumulative effect of enhancing the mean Rossby wave source. This activity is supported by the moisture flux biases noted in Fig. 14. The cumulative result is an SICZ, which provides similar forcing to the mean flow as that of the South Atlantic convergence zone (SACZ). In the observed atmosphere (ERA-Interim), the SACZ is more active and a source for Rossby waves propagating toward subtropical southern Africa. However, in these models (MANY\_WET, LAND\_FOCUS), Rossby wave growth is supported in situ over southern Africa with implications for the mean flow downstream.

## 7. Summary and conclusions

Climate projections are increasingly being used to inform adaptation planning, yet for many regions there is limited understanding of how models represent important climate processes. In this paper we seek to contribute fundamental understanding for southern Africa, by examining models' ability to simulate a dominant rainfall producing mechanism in the region: tropical temperate troughs (TTTs). All models analyzed generate TTTs and with similar synoptic circulation to reanalysis: TTTs form as part of a midlatitude wave that propagates northeastward into southern Africa. TTTs have a ridge–trough–ridge structure, and are sites of moisture convergence, with southeastward moisture flux, exporting water vapor poleward. The qualitative consistency in TTT structure between reanalysis and models is an encouraging result. However, while the models are capable of generating TTTs with a similar character to observed, there are large differences in the number of events generated, where they preferentially occur, and how much precipitation they contribute to the simulated rainfall climatology.

The models were divided into five groups according to their TTT behavior. The TOO\_FEW (green) group have a reasonable spatial distribution of TTTs, but underestimate their frequency. The MANY\_WET (navy) group generate large numbers of TTTs, with large amounts of precipitation, and these models have wet mean precipitation biases. The MANY\_DRY (yellow) group also generate too many TTTs, yet their precipitation climatology is relatively close to observed, since each TTT event contributes only a small amount of precipitation. The OCEAN\_FOCUS (purple) group are notable in their longitudinal location of TTTs: relatively few are generated over the continent, and more occur

over Madagascar and the Indian Ocean. The LAND\_FOCUS group have a qualitatively opposite bias in spatial distribution, with TTTs occurring almost exclusively over the continent, and very few in the western Indian Ocean.

The number of TTTs in each model is related to the mean tropical and subtropical OLR, a proxy for convective activity. Some models underestimate Congo Basin convection, and this is associated with too few TTTs over the continent. This result is supported by Hart et al. (2018b), who demonstrate that a convective-permitting model simulates more Congo Basin convection than its parameterized parent model, associated with a vastly improved TTT climatology. The preferred locus of tropical convection also seems to relate to the preferred location for TTT generation in models. Those models with weak Congo Basin convection also overestimate convective activity in the west equatorial Indian Ocean, and generate too many TTTs over the ocean.

Another important factor that covaries with TTT location is the northeast monsoon. Some models overestimate the northeasterly flow into the subcontinent and do not represent the northwesterly wind recurvature toward Madagascar, associated with an underestimate of Madagascan TTTs, and more frequent and wet continental events. As diagnosed by Barimalala et al. (2018), this bias is consistent with low model orography over Madagascar, and is also likely linked to a flattened Tanzanian Escarpment in models. Another feature connected to the intensity of continental TTTs is the Angola low. This feature has now been shown to relate to both mean precipitation over southern Africa (Munday and Washington 2017) and the intensity of TTTs.

The mean westerly flow supporting the wave disturbances necessary for TTT formation was shown to differ in subtle yet crucial ways between the model groupings. In particular, overly strong and zonally symmetric westerly flow across southern Africa diminished TTT activity over the continent. However, the model groupings that produced wet and frequent TTTs over the continent demonstrated zonally asymmetric in the mean flow associated with strong subtropical diabatic heating. These models produce an SICZ with a magnitude and impact on the mean flow that is more like the observed SACZ than that observed over southern Africa. This overly enhanced SICZ activity is likely to be self-reinforcing. Zonally asymmetric flow, perhaps initially a result of tropical convection, would support equatorward wave refraction near southern Africa. These waves would favor frequent triggering of deep convection supported by moisture fluxes in to the subtropics. Deep convection and associated subtropical diabatic heating would act as a Rossby wave source and reinforce the zonal asymmetry.

Small changes in the representation of any one of the factors diagnosed here—tropical convection, moisture fluxes modulated by model orography, midlatitude jet strength, and wave activity—would perturb this feedback loop and result in intermodel diversity of TTT simulation and climatologies.

The findings of this paper make three important contributions. First, they provide a thorough assessment of the fidelity with which climate models simulate a key southern African rainfall system, and thereby inform their applications in adaptation planning. The results suggest that models have the ability to simulate TTTs similar to those observed. However, the differences in the number, location, and intensity of events, related to fundamental differences in the spatial distribution of tropical convection, and variation in regional circulation features, suggests care should be taken in applying these models to examine future changes over southern Africa. Any projected change in TTT activity may be related to changes in biased regional circulation. Yet rather than discounting the future projections, these results may rather support improved process understanding of projected changes. If we can analyze future changes in TTTs, and why they are occurring, these findings, and model groupings, could help to put them in context and therefore assess confidence. This is the goal of our future work.

The second contribution of this work is to model development. It has sometimes been suggested that the simulation of tropical precipitation can only be improved by running models at a resolution that allows for convective parameterizations to be switched off. TTT climatologies, which we show are sensitive to tropical convection, depend strongly on the parameterization of convection (e.g., [Tozuka et al. 2014](#)). And indeed, [Hart et al. \(2018b\)](#) find that a convective-permitting simulation has a better representation of TTTs than a global or regional model with convective parameterization. However, the CMIP5 models are able to generate TTTs despite their convective parameterizations. This suggests potential to improve the simulation of TTTs before convective-permitting global climate simulations are routinely possible. Specifically, the results here suggest that more realistic orography is fundamental to simulate the southern African climate system.

Finally, this work has potential to contribute to our understanding of the real southern African climate system. The divergence between climate models is often seen as a burden, with respect to informing adaptation. However, the multitude of different physical representations of the southern African system is also a resource to better understand it. The range of TTT behaviors helps us to infer under what conditions more or fewer TTTs form and what factors are associated with more or

less intense TTTs. For example, analysis of CMIP5 suggests that OLR in the south of the Congo Basin has an important association with the number of continental TTTs. With further work, these results could help us to get a better grasp on how the Congo Basin is associated with TTTs in the real world.

*Acknowledgments.* This research is supported by the U.K. Natural Environment Research Council (NERC) and Department for International Development (DfID) funded UMFULA project (NE/M20207/1), and in part by the National Research Foundation of South Africa (Grant 115875). The authors thank three anonymous reviewers for their constructive comments. We acknowledge the World Climate Research Programme's Working Group on Coupled Modelling, which is responsible for CMIP, and we thank the climate modeling groups for producing and making available their model output. For CMIP the U.S. Department of Energy's Program for Climate Model Diagnosis and Intercomparison provides coordinating support and led development of software infrastructure in partnership with the Global Organization for Earth System Science Portals. The NOAA CDR OLR data were originally developed by Hai-Tien Lee and colleagues for NOAA's CDR Program. We gratefully acknowledge the creators of the TRMM, GTOPO30, and ERAI datasets.

*Data availability statement.* CMIP5 data are publicly available for noncommercial research and educational purposes and can be downloaded from <https://pcmdi.llnl.gov/>. The Outgoing Longwave Radiation–Daily CDR used in this study can be acquired from NOAA's National Centers for Environmental Information (<http://www.ncei.noaa.gov>). The TRMM data used here are available at <https://doi.org/10.5067/TRMM/TMPA/3H/7>. ERA-Interim data are available at <https://www.ecmwf.int/en/forecasts/datasets/reanalysis-datasets/era-interim>. The GTOPO30 global digital elevation model data are available from the U.S. Geological Survey: <http://earthexplorer.usgs.gov/>. The code used to generate the TTT event sets and for all analysis used in this paper are available at <https://github.com/rjames-at-rwjames/MetBot>.

## REFERENCES

- Barimalala, R., F. Desbiolles, R. C. Blamey, and C. Reason, 2018: Madagascar influence on the south Indian Ocean convergence zone, the Mozambique channel trough and southern African rainfall. *Geophys. Res. Lett.*, **45**, 11 380–11 389, <https://doi.org/10.1029/2018GL079964>.
- Bopape, M. J. M., and Coauthors, 2019: Programme for the development of weather and climate numerical modelling systems in South Africa. *S. Afr. J. Sci.*, **115**, 10–13, <https://doi.org/10.17159/SAJS.2019/5779>.

- Collins, M., and Coauthors, 2013: Long-term climate change: Projections, commitments and irreversibility. *Climate Change 2013: The Physical Science Basis*, T. F. Stocker et al., Eds., Cambridge University Press, 1029–1136.
- Cook, C., C. Reason, and B. Hewitson, 2004: Wet and dry spells within particularly wet and dry summers in the South African summer rainfall region. *Climate Res.*, **26**, 17–31, <https://doi.org/10.3354/cr026017>.
- Creese, A., and R. Washington, 2016: Using qflux to constrain modeled Congo Basin rainfall in the CMIP5 ensemble. *J. Geophys. Res. Atmos.*, **121**, 13 415–13 442, <https://doi.org/10.1002/2016JD025596>.
- Cr  tat, J., B. Pohl, B. Dieppo  s, S. Berthou, and J. Pergaud, 2018: The Angola low: Relationship with southern African rainfall and ENSO. *Climate Dyn.*, **52**, 1783–1803, <https://doi.org/10.1007/s00382-018-4222-3>.
- Dee, D. P., and Coauthors, 2011: The ERA-Interim reanalysis: Configuration and performance of the data assimilation system. *Quart. J. Roy. Meteor. Soc.*, **137**, 553–597, <https://doi.org/10.1002/qj.828>.
- ECMWF, 2009: ERA-Interim project. Research Data Archive at the National Center for Atmospheric Research, Computational and Information Systems Laboratory, accessed 21 January 2015, <https://doi.org/10.5065/D6CR5RD9>.
- Eyring, V., S. Bony, G. A. Meehl, C. A. Senior, B. Stevens, R. J. Stouffer, and K. E. Taylor, 2016: Overview of the Coupled Model Intercomparison Project Phase 6 (CMIP6) experimental design and organization. *Geosci. Model Dev.*, **9**, 1937–1958, <https://doi.org/10.5194/gmd-9-1937-2016>.
- Fauchereau, N., B. Pohl, C. J. C. Reason, M. Rouault, and Y. Richard, 2009: Recurrent daily OLR patterns in the Southern Africa/Southwest Indian Ocean region, implications for South African rainfall and teleconnections. *Climate Dyn.*, **32**, 575–591, <https://doi.org/10.1007/s00382-008-0426-2>.
- Gleckler, P. J., K. E. Taylor, and C. Doutriaux, 2008: Performance metrics for climate models. *J. Geophys. Res.*, **113**, D06104, <https://doi.org/10.1029/2007JD008972>.
- Harrison, M. S. J., 1984: A generalized classification of South African summer rain-bearing synoptic systems. *J. Climatol.*, **4**, 547–560, <https://doi.org/10.1002/joc.3370040510>.
- Hart, N. C. G., C. J. C. Reason, and N. Fauchereau, 2010: Tropical–extratropical interactions over southern Africa: Three cases of heavy summer season rainfall. *Mon. Wea. Rev.*, **138**, 2608–2623, <https://doi.org/10.1175/2010MWR3070.1>.
- , —, and —, 2012: Building a tropical–extratropical cloud band metbot. *Mon. Wea. Rev.*, **140**, 4005–4016, <https://doi.org/10.1175/MWR-D-12-00127.1>.
- , —, and —, 2013: Cloud bands over southern Africa: Seasonality, contribution to rainfall variability and modulation by the MJO. *Climate Dyn.*, **41**, 1199–1212, <https://doi.org/10.1007/s00382-012-1589-4>.
- , R. Washington, and C. J. C. Reason, 2018a: On the likelihood of tropical–extratropical cloud bands in the south Indian convergence zone during ENSO events. *J. Climate*, **31**, 2797–2817, <https://doi.org/10.1175/JCLI-D-17-0221.1>.
- , —, and R. Stratton, 2018b: Stronger local overturning in convective-permitting regional climate model improves the simulation of subtropical annual cycle. *Geophys. Res. Lett.*, **45**, 11 334–11 342, <https://doi.org/10.1029/2018GL079563>.
- Hewitson, B., K. Waagsaether, J. Wohland, K. Kloppe  s, and T. Kara, 2017: Climate information websites: An evolving landscape. *Wiley Interdiscip. Rev. Climate Change*, **8**, e470, <https://doi.org/10.1002/wcc.470>.
- Hewitt, C., S. Mason, and D. Walland, 2012: The global framework for climate services. *Nat. Climate Change*, **2**, 831–832, <https://doi.org/10.1038/nclimate1745>.
- Hirons, L., and A. Turner, 2018: The impact of Indian Ocean mean-state biases in climate models on the representation of the East African short rains. *J. Climate*, **31**, 6611–6631, <https://doi.org/10.1175/JCLI-D-17-0804.1>.
- Hoskins, B. J., and D. J. Karoly, 1981: The steady linear response of a spherical atmosphere to thermal and orographic forcing. *J. Atmos. Sci.*, **38**, 1179–1196, [https://doi.org/10.1175/1520-0469\(1981\)038<1179:TSLROA>2.0.CO;2](https://doi.org/10.1175/1520-0469(1981)038<1179:TSLROA>2.0.CO;2).
- , and T. Ambrizzi, 1993: Rossby wave propagation on a realistic longitudinally varying flow. *J. Atmos. Sci.*, **50**, 1661–1671, [https://doi.org/10.1175/1520-0469\(1993\)050<1661:RWPOAR>2.0.CO;2](https://doi.org/10.1175/1520-0469(1993)050<1661:RWPOAR>2.0.CO;2).
- Howard, E., and R. Washington, 2018: Characterizing the synoptic expression of the Angola low. *J. Climate*, **31**, 7147–7165, <https://doi.org/10.1175/JCLI-D-18-0017.1>.
- Huffman, G. J., and Coauthors, 2007: The TRMM Multisatellite Precipitation Analysis (TMPA): Quasi-global, multiyear, combined-sensor precipitation estimates at fine scales. *J. Hydrometeorol.*, **8**, 38–55, <https://doi.org/10.1175/JHM560.1>.
- , E. F. Stocker, D. T. Bolvin, E. J. Nelkin, and R. F. Adler, 2014: Tropical Rainfall Measuring Mission (TRMM) 3B42 research derived daily product v.7. NASA/GSFC, accessed 13 January 2015, <https://pmm.nasa.gov/data-access/downloads/trmm>.
- IPCC, 2012: *Managing the Risks of Extreme Events and Disasters to Advance Climate Change Adaptation: Special Report of the Intergovernmental Panel on Climate Change*. Cambridge University Press, 582 pp., [https://www.ipcc.ch/site/assets/uploads/2018/03/SREX\\_Full\\_Report-1.pdf](https://www.ipcc.ch/site/assets/uploads/2018/03/SREX_Full_Report-1.pdf).
- James, R., and R. Washington, 2013: Changes in African temperature and precipitation associated with degrees of global warming. *Climatic Change*, **117**, 859–872, <https://doi.org/10.1007/s10584-012-0581-7>.
- , —, and D. P. Rowell, 2014: African climate change uncertainty in perturbed physics ensembles: Implications of global warming to 4  C and beyond. *J. Climate*, **27**, 4677–4692, <https://doi.org/10.1175/JCLI-D-13-00612.1>.
- , and Coauthors, 2018: Evaluating climate models with an African lens. *Bull. Amer. Meteor. Soc.*, **99**, 313–336, <https://doi.org/10.1175/BAMS-D-16-0090.1>.
- Kanamitsu, M., W. Ebisuzaki, J. Woollen, S. K. Yang, J. J. Hnilo, M. Fiorino, and G. L. Potter, 2002: NCEP–DOE AMIP-II Reanalysis (R-2). *Bull. Amer. Meteor. Soc.*, **83**, 1631–1643, <https://doi.org/10.1175/BAMS-83-11-1631>.
- Knutti, R., R. Furrer, C. Tebaldi, J. Cermak, and G. A. Meehl, 2010: Challenges in combining projections from multiple climate models. *J. Climate*, **23**, 2739–2758, <https://doi.org/10.1175/2009JCLI3361.1>.
- Lazenby, M., M. Todd, and Y. Wang, 2016: Climate model simulation of the south Indian Ocean convergence zone: Mean state and variability. *Climate Res.*, **68**, 59–71, <https://doi.org/10.3354/cr01382>.
- Lee, H.-T., 2014: Climate Algorithm Theoretical Basis Document (C-ATBD): Outgoing Longwave Radiation (OLR)–Daily. Tech. Rep. CDRP-ATBD-0526, NOAA’s Climate Data Record (CDR) Program, 46 pp., <http://www1.ncdc.noaa.gov/pub/data/sds/cdr/CDRs/Outgoing%20Longwave%20Radiation20-%20Daily/AlgorithmDescription.pdf>.
- , and Coauthors, 2011: NOAA Climate Data Record (CDR) of daily outgoing longwave radiation (OLR), version 1.2. NOAA National Climatic Data Center, accessed 13 January 2015, <https://doi.org/10.7289/V5SJ1HH2>.
- Lindesay, J. A., 1988: South African rainfall, the Southern Oscillation and a Southern Hemisphere semi-annual cycle. *Int. J. Climatol.*, **8**, 17–30, <https://doi.org/10.1002/joc.3370080103>.

- Livezey, R. E., and W. Y. Chen, 1983: Statistical field significance and its determination by Monte Carlo techniques. *Mon. Wea. Rev.*, **111**, 46–59, [https://doi.org/10.1175/1520-0493\(1983\)111%3C0046:SFSAD%3E2.0.CO;2](https://doi.org/10.1175/1520-0493(1983)111%3C0046:SFSAD%3E2.0.CO;2).
- Macron, C., B. Pohl, Y. Richard, and M. Bessafi, 2014: How do tropical temperate troughs form and develop over southern Africa? *J. Climate*, **27**, 1633–1647, <https://doi.org/10.1175/JCLI-D-13-00175.1>.
- Manhique, A. J., C. J. C. Reason, L. Rydberg, and N. Fauchereau, 2011: ENSO and Indian Ocean sea surface temperatures and their relationships with tropical temperate troughs over Mozambique and the southwest Indian Ocean. *Int. J. Climatol.*, **31** (1), 1–13, <https://doi.org/10.1002/joc.2050>.
- , —, B. Silinto, J. Zucula, I. Raiva, F. Congolo, and A. F. Mavume, 2015: Extreme rainfall and floods in southern Africa in January 2013 and associated circulation patterns. *Nat. Hazards*, **77**, 679–691, <https://doi.org/10.1007/s11069-015-1616-y>.
- Mulenga, H. M., M. Rouault, and C. J. C. Reason, 2003: Dry summers over northeastern South Africa and associated circulation anomalies. *Climate Res.*, **25**, 29–41, <https://doi.org/10.3354/cr025029>.
- Munday, C., and R. Washington, 2017: Circulation controls on southern African precipitation in coupled models: The role of the Angola low. *J. Geophys. Res. Atmos.*, **122**, 861–877, <https://doi.org/10.1002/2016JD025736>.
- , and —, 2018: Systematic climate model rainfall biases over southern Africa: Links to moisture circulation and topography. *J. Climate*, **31**, 7533–7548, <https://doi.org/10.1175/JCLI-D-18-0008.1>.
- , and —, 2019: Controls on the diversity in climate model projections of early summer drying over southern Africa. *J. Climate*, **32**, 3707–3725, <https://doi.org/10.1175/JCLI-D-18-0463.1>.
- Niang, I., O. C. Ruppel, M. A. Abdrabo, A. Essel, C. Lennard, J. Padgham, and P. Urquhart, 2014: Africa. *Climate Change 2014: Impacts, Adaptation, and Vulnerability. Part B: Regional Aspects*, V. R. Barros et al., Eds., Cambridge University Press, 1199–1265.
- Nissan, H., L. Goddard, E. C. de Perez, J. Furlow, W. Baethgen, M. C. Thomson, and S. J. Mason, 2019: On the use and misuse of climate change projections in international development. *Wiley Interdiscip. Rev. Climate Change*, **10**, e579, <https://doi.org/10.1002/wcc.579>.
- Ratna, S. B., S. Behera, J. V. Ratnam, K. Takahashi, and T. Yamagata, 2013: An index for tropical temperate troughs over southern Africa. *Climate Dyn.*, **41**, 421–441, <https://doi.org/10.1007/s00382-012-1540-8>.
- Reichler, T., and J. Kim, 2008: How well do coupled models simulate today's climate? *Bull. Amer. Meteor. Soc.*, **89**, 303–311, <https://doi.org/10.1175/BAMS-89-3-303>.
- Rouault, M., P. Florenchie, N. Fauchereau, and C. J. C. Reason, 2003: South East tropical Atlantic warm events and southern African rainfall. *Geophys. Res. Lett.*, **30**, 8009, <https://doi.org/10.1029/2002GL014840>.
- Sardeshmukh, P. D., and B. J. Hoskins, 1988: The generation of global rotational flow by steady idealized tropical divergence. *J. Atmos. Sci.*, **45**, 1228–1251, [https://doi.org/10.1175/1520-0469\(1988\)045<1228:TGOGRF>2.0.CO;2](https://doi.org/10.1175/1520-0469(1988)045<1228:TGOGRF>2.0.CO;2).
- Schaller, N., I. Mahlstein, J. Cermak, and R. Knutti, 2011: Analyzing precipitation projections: A comparison of different approaches to climate model evaluation. *J. Geophys. Res.*, **116**, D10118, <https://doi.org/10.1029/2010JD014963>.
- Shongwe, M. E., G. J. van Oldenborgh, B. J. J. M. van den Hurk, B. de Boer, C. S. Coelho, and M. K. van Aalst, 2009: Projected changes in mean and extreme precipitation in Africa under global warming. Part I: Southern Africa. *J. Climate*, **22**, 3819–3837, <https://doi.org/10.1175/2009JCLI2317.1>.
- Taljaard, J. J., 1996: Atmospheric circulation systems, synoptic climatology and weather phenomena of South Africa, Part 6: Rainfall in South Africa. South African Weather Bureau Tech. Paper 32, 100 pp.
- Taylor, K. E., R. J. Stouffer, and G. A. Meehl, 2012: An overview of CMIP5 and the experiment design. *Bull. Amer. Meteor. Soc.*, **93**, 485–498, <https://doi.org/10.1175/BAMS-D-11-00094.1>.
- Tennant, W., 2003: An assessment of intraseasonal variability from 13-yr GCM simulations. *Mon. Wea. Rev.*, **131**, 1975–1991, [https://doi.org/10.1175/1520-0493\(2003\)131<1975:AAOIVF>2.0.CO;2](https://doi.org/10.1175/1520-0493(2003)131<1975:AAOIVF>2.0.CO;2).
- Todd, M., and R. Washington, 1998: Extreme daily rainfall in southern African and southwest Indian Ocean tropical-temperate links. *S. Afr. J. Sci.*, **94**, 64–70.
- , and —, 1999: Circulation anomalies associated with tropical-temperate troughs in southern Africa and the southwest Indian Ocean. *Climate Dyn.*, **15**, 937–951, <https://doi.org/10.1007/s003820050323>.
- , —, and P. I. Palmer, 2004: Water vapour transport associated with tropical-temperate trough systems over southern Africa and the southwest Indian Ocean. *Int. J. Climatol.*, **24**, 555–568, <https://doi.org/10.1002/joc.1023>.
- Tozuka, T., B. J. Abiodun, and F. Engelbrecht, 2014: Impacts of convection schemes on simulating tropical-temperate troughs over southern Africa. *Climate Dyn.*, **42**, 433–451, <https://doi.org/10.1007/s00382-013-1738-4>.
- van der Wiel, K., A. J. Matthews, D. P. Stevens, and M. M. Joshi, 2015: A dynamical framework for the origin of the diagonal South Pacific and South Atlantic convergence zones. *Quart. J. Roy. Meteor. Soc.*, **141**, 1997–2010, <https://doi.org/10.1002/qj.2508>.
- Vaughan, C., and S. Dessai, 2014: Climate services for society: Origins, institutional arrangements, and design elements for an evaluation framework. *Wiley Interdiscip. Rev.: Climate Change*, **5**, 587–603, <https://doi.org/10.1002/wcc.290>.
- Vigaud, N., B. Pohl, and J. Cr  tat, 2012: Tropical-temperate interactions over southern Africa simulated by a regional climate model. *Climate Dyn.*, **39**, 2895–2916, <https://doi.org/10.1007/s00382-012-1314-3>.
- Washington, R., and M. Todd, 1999: Tropical-temperate links in southern African and southwest Indian Ocean satellite-derived daily rainfall. *Int. J. Climatol.*, **19**, 1601–1616, [https://doi.org/10.1002/\(SICI\)1097-0088\(19991130\)19:14<1601::AID-JOC407>3.0.CO;2-0](https://doi.org/10.1002/(SICI)1097-0088(19991130)19:14<1601::AID-JOC407>3.0.CO;2-0).
- Watterson, I. G., J. Bathols, and C. Heady, 2014: What influences the skill of climate models over the continents? *Bull. Amer. Meteor. Soc.*, **95**, 689–700, <https://doi.org/10.1175/BAMS-D-12-00136.1>.
- Widlansky, M. J., P. J. Webster, and C. D. Hoyos, 2011: On the location and orientation of the South Pacific convergence zone. *Climate Dyn.*, **36**, 561–578, <https://doi.org/10.1007/s00382-010-0871-6>.
- Wilks, D., 2016: “The stippling shows statistically significant grid points”: How research results are routinely overstated and overinterpreted, and what to do about it. *Bull. Amer. Meteor. Soc.*, **97**, 2263–2273, <https://doi.org/10.1175/BAMS-D-15-00267.1>.
- World Bank, 2012: Turn down the heat: Why a 4°C warmer world must be avoided. World Bank, 106 pp., <http://documents1.worldbank.org/curated/en/865571468149107611/pdf/NonAsciiFileName0.pdf>.